Classification and sound generation of two-dimensional interaction of two Taylor vortices

Shuhai Zhang[1], Hu Li[2], Xuliang Liu[3], Hanxin Zhang[4] and Chi-Wang Shu[5]

Abstract

Two-dimensional interaction between two Taylor vortices is simulated systematically through solving the two-dimensional, unsteady compressible Navier-Stokes equations using a fifth order weighted essentially nonoscillatory finite difference scheme. The main purpose of this study is to reveal the mechanism of sound generation in two-dimensional interaction of two Taylor vortices. Based on an extensive parameter study on the evolution of the vorticity field, we classify the interaction of two Taylor vortices into four types. The first type is the interaction of two counter-rotating vortices with similar strengths. The second type is the interaction of two co-rotating vortices without merging. The third type is the merging of two co-rotating vortices. The fourth type is the interaction of two vortices with a large difference in their strengths or scales. The mechanism of sound generation is analyzed.

Key Words: WENO scheme, sound wave, Taylor vortex.

[1]State Key Laboratory of Aerodynamics, China Aerodynamics Research and Development Center, Mianyang, Sichuan 621000, China. E-mail: shzhang@skla.cardc.cn. Research supported by the Chinese National Natural Science Foundation grants 11172317, 91016001 and 973 program 2009CB724104.

[2]State Key Laboratory of Aerodynamics, China Aerodynamics Research and Development Center, Mianyang, Sichuan 621000, China. E-mail: Hli@skla.cardc.cn.

[3]State Key Laboratory of Aerodynamics, China Aerodynamics Research and Development Center, Mianyang, Sichuan 621000, China. E-mail: xlliu@foxmail.com.

[4]China Aerodynamics Research and Development Center, Mianyang, Sichuan 621000, China. Research supported by the Chinese National Natural Science Foundation grant 91016001.

[5]Division of Applied Mathematics, Brown University, Providence, RI 02912, USA. E-mail: shu@dam.brown.edu. Research partially supported by ARO grant W911NF-11-1-0091 and NSF grant DMS-1112700.

1 Introduction

Since the pioneering work of Lighthill [1] in 1952 on aerodynamic sound generation, the sound generated by unsteady flows has received increasing attention. Many theories have been developed [2, 3, 4, 5, 6, 7, 8, 9]. Typical examples include the vortex sound theory of Powell [2], the wave antenna theory of Crow [3], the instability wave model of Ffowcs Williams and Kempton [4] and the stagnation enthalpy theory of Doak [5]. These theories do offer better understandings to the generation of aerodynamic noise and provide good methods in engineering to calculate the noise generated by unsteady flows such as shear layer [6, 10], jet [7, 8, 11], wake [12] and airframes [13]. However, from the earliest stress tensor theory of Lighthill [1] to the recent stagnation enthalpy theory of Doak [5], the theoretical sound sources are rather abstract and difficult to measure. See [14, 15, 16, 17] for discussions on turbulence measurements for sound source modeling.

It is well known that sound can be generated by turbulent flows. However, owing to the difficulty in studying turbulent flows, it is necessary to first study simpler flow models. Vortices are building blocks of turbulent flows. In compressible turbulence, the interaction among these vortices plays an important role.

Mitchell et al. [18] studied the pairing process of two Gaussian vortices by a direct numerical simulation. The sound generated by the leapfrogging (referring to two or more vortices or vortex structures rotating around) and pairing is revealed. It is found that strong noise is generated at the instant of vortex merging. Besides, the sound wave obtained by the direct numerical simulation and the traditional theory is compared. In the direct numerical simulation for a plane mixing layer [10] and an axisymmetric jet [19], it is found that the vortex pairing is a key mechanism of sound generation in shear layer turbulent flows. However, the Gaussian vortex is just one type of vortices. There may be features of vortex interactions in real turbulent flows that can not be described by Gaussian vortices. Therefore, it is worthwhile to study the interaction of two Taylor vortices. For example, in the wake of a school of fish [20, 21], vortex dipoles often are formed from the interaction of two counter-rotating vortices, which are similar to those in the interaction of two counter-rotating Taylor vortices [22, 23]. Tang and Ko [24, 25] studied the interaction of inviscid two-dimensional vortices by the method of contour dynamics and the mechanism of sound generation by the vortex sound theory. It is found that the motions of the velocity centroid and the unsteady deformation of the vortex cores are the sources of sound generated in the interaction. The sound wave generated by the interaction of two identical vortices results from the leapfrogging and coalescence, while the sound wave generated by the interaction of unequal vortices results from leapfrogging, shearing and tearing processes. The advantage of using contour dynamics is that the vortices and their boundaries are explicitly defined, which allows the Möhring source terms [18, 26] to be easily broken down into contributions from each vortex. However, real fluid effects, such as viscosity and nearfield compressibility, are obviously ignored in this approach, and such effects may have direct or indirect consequences on aeroacoustics. Non-uniform distributions of vorticity can not be simulated, and therefore the effect of this non-uniformity on the magnitude of the acoustic field components cannot be assessed.

Using a vortex particle method and direct numerical simulation for two-dimensional full Navier-Stokes equations, Eldredge [27] studied the dynamics and sound generation of viscous two-dimensional leapfrogging vortex pairs. The relationship between the deformation of the vortex core and the filament stripped from the outer region of the vortex is analyzed. It is demonstrated that both the initial distribution of the vortex and the viscous diffusion are crucially important for the sound generation.

Shock vortex interaction is another simple model to study the sound generation of compressible turbulent flow due to the coexistence of shock waves and vortices in compressible turbulence. Compared to the study on the interaction of vortices, there are more studies on shock vortex interaction, which contains the interaction between a shock wave and a single vortex and the interaction between a shock wave and a pair of vortices. We will not discuss this issue in detail and refer the readers to the references [22, 23, 28, 29, 30, 31, 32].

In fact, both vortex-vortex interaction and shock-vortex interaction may take place at the same time. In past few years, we have studied the interaction between a shock wave and a strong Taylor vortex [31] and the interaction between a shock wave and a pair of Taylor vortices [22, 23]. We have found that the interaction of a shock wave and a strong vortex has multistage feature and predicted that the sound generated has also multistage feature, which has been demonstrated by Chatterjee and Vijayaraj [33]. For the interaction of a shock and a pair of Taylor vortices, we have found that there are two regimes of sound generation in the interaction. The first regime is linear which corresponds to the shock interaction with two isolated vortices, in which the sound wave generated by the interaction between the shock wave and a pair of vortices equals to the linear combination of the sound waves generated by the interactions between the same shock wave and each vortex. The second regime is nonlinear which corresponds to the shock interaction with a coupled vortex pair, in which the sound wave comes from two processes. One is the vortex coupling, and the second is the interaction between the shock wave and the coupled vortex pair. The work in this paper is an extension of our previous work in [23]. Using a fifth order weighted essentially nonoscillatory (WENO) finite difference scheme [34], we systematically study the interaction between two Taylor vortices through simulating the two-dimensional unsteady Navier-Stokes equations. Our purpose is to study the mechanism of sound generation by the interaction of two Taylor vortices to reveal the mechanism of sound generation of the first process in the second regime of the interaction of a shock and a pair of strong vortices [23]. The effect of the strength of the vortices and the geometry parameters are studied systematically. The mechanism of sound generation is analyzed by comparing the characteristics of sound waves and the dynamic process of two-dimensional interaction of two Taylor vortices.

This paper is organized as follows. In Section 2, the numerical method and the physical model are briefly introduced. In Section 3, we present our simulation results and provide a detailed discussion for the sound generation. In Section 4, we revisit the interaction between two Gaussian vortices to show the difference in the sound generation between two different types of vortices. In Section 5, the classification for the two-dimensional interaction of two Taylor vortices is partly demonstrated by a decaying two-dimensional homogeneous turbulence through direct numerical simulation. Section 6 contains our concluding remarks.

2 The physical model for the interaction of two Taylor vortices

2.1 The numerical method

The fifth order finite difference WENO scheme developed by Jiang and Shu [34] is used to simulate the following two-dimensional unsteady compressible Navier-Stokes equations.

$$U_t + F(U)_x + G(U)_y = \frac{1}{Re}(F_\nu(U)_x + G_\nu(U)_y) \tag{1}$$

where $U = (\rho, \rho u, \rho v, e)^T$, $F(U) = (\rho u, \rho u^2 + p, \rho uv, u(e+p))^T$, $G(U) = (\rho v, \rho uv, \rho v^2 + p, v(e+p))^T$, $F_\nu(U) = (0, \tau_{xx}, \tau_{xy}, u\tau_{xx} + v\tau_{xy} + q_x)^T$, $G_\nu(U) = (0, \tau_{xy}, \tau_{yy}, u\tau_{xy} + v\tau_{yy} + q_y)^T$. Here ρ is the density, (u, v) is the velocity, e is the total energy, p is the pressure, which is related to the total energy by $e = \frac{p}{\gamma-1} + \frac{1}{2}\rho(u^2+v^2)$, the ratio of specific heats $\gamma = 1.4$. Re is the Reynolds number defined by $Re = \rho_\infty a_\infty R/\mu_\infty$, where ρ_∞, a_∞ and μ_∞ are the density, sound speed and viscosity for the free stream and R is the radius of the vortex core of the larger or stronger Taylor vortex defined by the distance from the vortex center to the location where the tangential velocity attains its maximum. τ_{ij} and q_j (where $i, j = 1$ for x and $i, j = 2$ for y) are the stress tensor and the heat flux respectively and are given as:

$$\tau_{ij} = \mu\left(\frac{\partial u_i}{\partial x_j} + \frac{\partial u_j}{\partial x_i} - \frac{2}{3}\delta_{ij}\frac{\partial u_k}{\partial x_k}\right), \qquad q_j = \frac{\mu}{(\gamma-1)Pr}\frac{\partial T}{\partial x_j}$$

where $Pr = 0.75$ is the Prandtl number, $\mu = T^{\frac{3}{2}}\frac{1+c}{T+c}$ is the viscosity computed by the Sutherland law, with $c = 110.4/T_\infty$ and $T_\infty = 300$, and $T = \gamma p/\rho$ is the temperature.

The nonlinear first derivative terms of the Navier-Stokes equations are discretized by the fifth order finite difference WENO scheme. It has fifth order accuracy in smooth regions. The solution is essentially non-oscillatory and gives sharp shock transitions near discontinuities. We refer to [34] and [35] for more details.

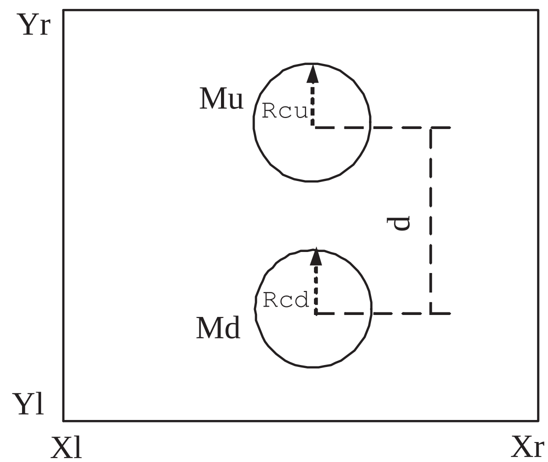

Figure 1: Schematic diagram of the flow model for the interaction of two Taylor vortices.

The viscous terms are discretized by a fourth order central difference scheme and the time derivative is discretized by the third order TVD Runge-Kutta method of Shu and Osher [36]. We again refer to [35] for more details.

2.2 The physical model for the interaction of two Taylor vortices

Figure 1 is the schematic diagram of the flow model for the interaction of two Taylor vortices. M_{vu} and M_{vd} are the strengths of the upper and lower vortices respectively. d is the initial separation distance of the two vortices. The computational domain is prescribed to be rectangular $x_l < x < x_r$, $y_l < y < y_r$. In our simulation, we choose $x_l = y_l = -220$ and $x_r = y_r = 220$.

The initial value of a single Taylor vortex [31, 35, 37] is set as follows:

tangential velocity: $u_\theta(r) = M_v r e^{(1-r^2)/2}$,

radial velocity: $u_r = 0$,

pressure: $p(r) = \frac{1}{\gamma}[1 - \frac{\gamma-1}{2} M_v^2 e^{1-r^2}]^{\frac{\gamma}{\gamma-1}}$,

density: $\rho(r) = [1 - \frac{\gamma-1}{2} M_v^2 e^{1-r^2}]^{\frac{1}{\gamma-1}}$

where $r = \sqrt{(x-x_v)^2 + (y-y_v)^2}/R_c$. (x_v, y_v) is the center of the initial vortex. R_c is the critical radius of a single vortex for which the vortex has the maximum strength. M_v is the strength of a single Taylor vortex. The initial flow field for the interaction of two vortices is prescribed by the superposition of the flow field produced by each single vortex. In our simulation, the strengths of the upper (M_{vu}) and the lower vortices (M_{vd}) are chosen from 0.01, 0.2, 0.25, 0.45, 0.5, 0.75 and 0.8. The separation distance of the two vortices is set to be d = 2, 2.2, 3, 4, 6 or 8. The initial locations of the upper and lower vortices are set to be $(x_u, y_u) = (0., \frac{1}{2}d)$ and $(x_d, y_d) = (0., -\frac{1}{2}d)$ respectively. The radius of upper and bottom vortices R_{cu} and R_{cd} are set to be $R_{cu} = R_{cd} = 1.0$ or $R_{cu} = 1.0$ and $R_{cd} = 0.2$. The computational cases consist of an extensive list of combinations of above listed parameters, which contain more than one hundred numerical cases. Throughout these computations, a Reynolds number of 800 is used. Only representative cases are shown to save space and to highlight the main conclusions.

After a grid convergence study to confirm sufficient grid resolution, we use an uniform mesh with the grid density of 6000×6000, which can offer numerically resolved solution for the vorticity field and sound waves under study.

3 Classification and sound generation of the two-dimensional interaction of two Taylor vortices

3.1 Classification of the two-dimensional interaction of two Taylor vortices

The interaction of two Taylor vortices has a close relationship with four parameters that contain the rotating direction, the strength, the radius and the initial separation distance of the two vortices. Based on a wide range parameter study and the evolution of the vorticity field, we classify the interaction into four types. They are the interaction of two counter-rotating vortices with similar strengths, the interaction of two co-rotating vortices without merging, the merging of two co-rotating vortices and the interaction between two Taylor vortices with a large difference in their strengths or scales.

Type I: The interaction of two counter-rotating vortices with similar strengths

The interaction between two counter-rotating vortices with similar strengths will result in a new flow structure and will generate sound waves if they are close enough. Figure 2 is the evolution of the vorticity in the interaction of two counter-rotating vortices. The strengths of both the upper and the lower vortex are the same with $M_{vu} = -0.5$ and $M_{vd} = 0.5$. They have the same radius with $R_{cu} = R_{cd} = 1$. The upper vortex rotates clockwise and the lower vortex rotates in the opposite direction. The initial distance of the two vortices is $d = 4$. As can be seen from Figure 2(a), the initial Taylor vortex has two layers, the inner layer and the outer layer. The sign of the vorticity is opposite in the inner layer and the outer layer. The interaction results in a significant change in their shapes. The vortex cores are pressed to an approximately elliptical shape from the initially circular shape and they gradually form a vortex dipole, which is advected to the left by the induced velocity. The outer layers move toward the symmetry line and gradually separate from the vortex core. They form a weak vortex dipole which moves to the right.

In practice, the strengths of two vortices are often not equal exactly, which results in the strengths of two vortex cores of each vortex dipole being not equal. Hence, the evolved vortex dipoles are often asymmetric and the trace of the vortex dipoles are curved. Figure 3 contains the evolution of two Taylor vortices with a slight difference in their strengths. The strength of the upper vortex $M_{vu} = -0.5$ and it is $M_{vd} = 0.45$ for the lower vortex. This kind of slightly asymmetric vortex dipoles often appear in the wake of a school of fish [20, 21]. The evolution of the interaction of two Taylor vortices is similar to that of the Taylor-type vortex pair coupling [38] and is observed in the experiment by Schmidt et al. [39].

Type II: The interaction of two co-rotating vortices without merging

There are two types in the interaction of two co-rotating vortices. The first type is the interaction of two co-rotating vortices without merging. The second type is the merging of two co-rotating vortices.

Figure 4 contains the evolution of the vorticity field in the interaction of two co-rotating

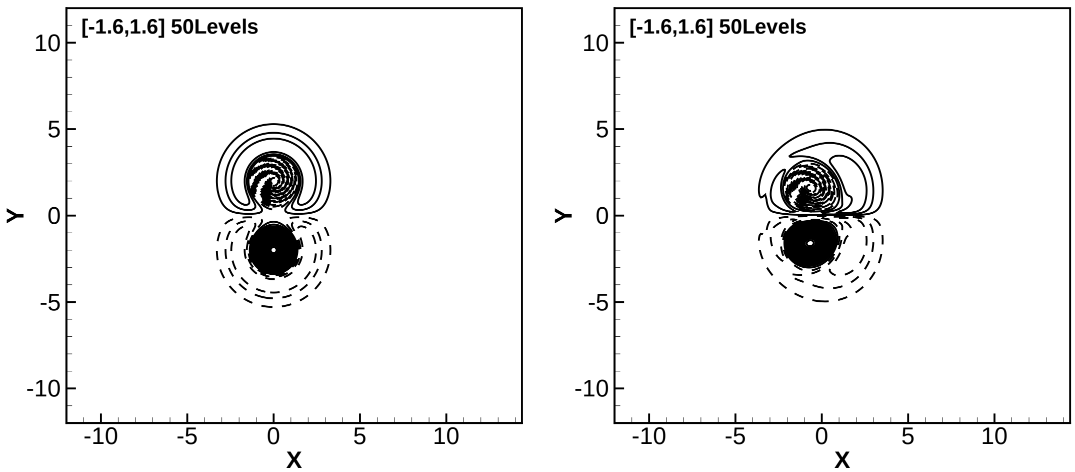

(a) $t = 0$ (b) $t = 20$

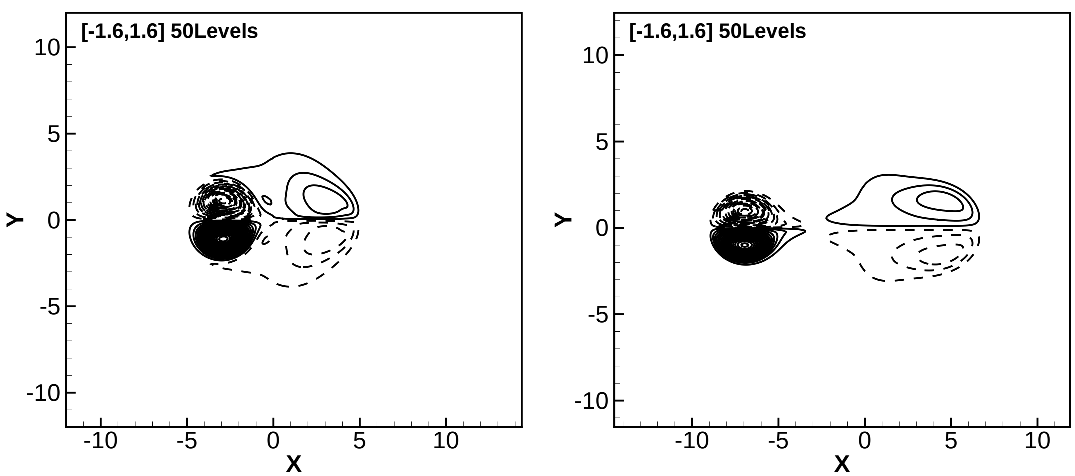

(c)$t = 40$ (d) $t = 60$

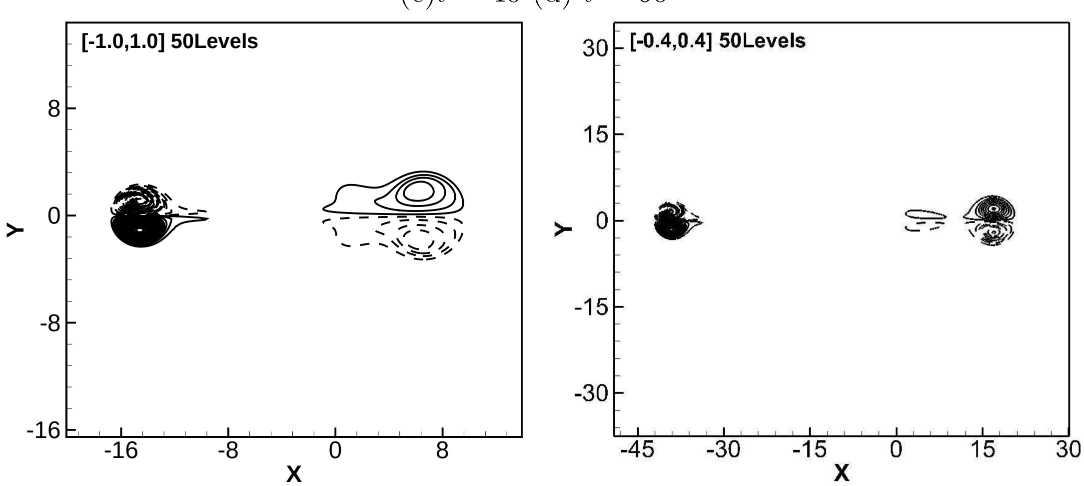

(e)$t = 100$ (f) $t = 300$

Figure 2: The evolution of the vorticity field in the interaction of two counter-rotating vortices in the case of $M_{vu} = -0.5$, $M_{vd} = 0.5$, $d = 4$ and $R_{cu} = R_{cd} = 1$.

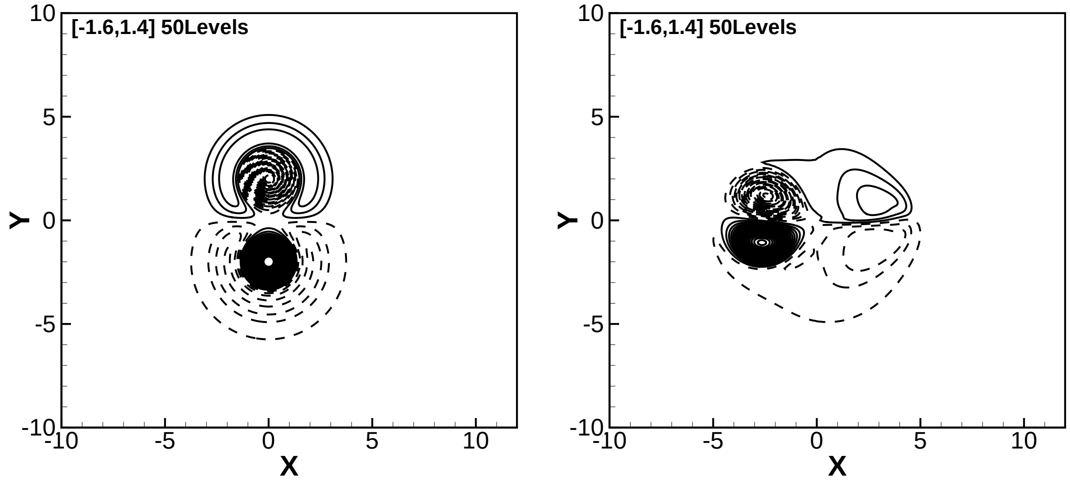

(a) $t = 0$ (b) $t = 40$

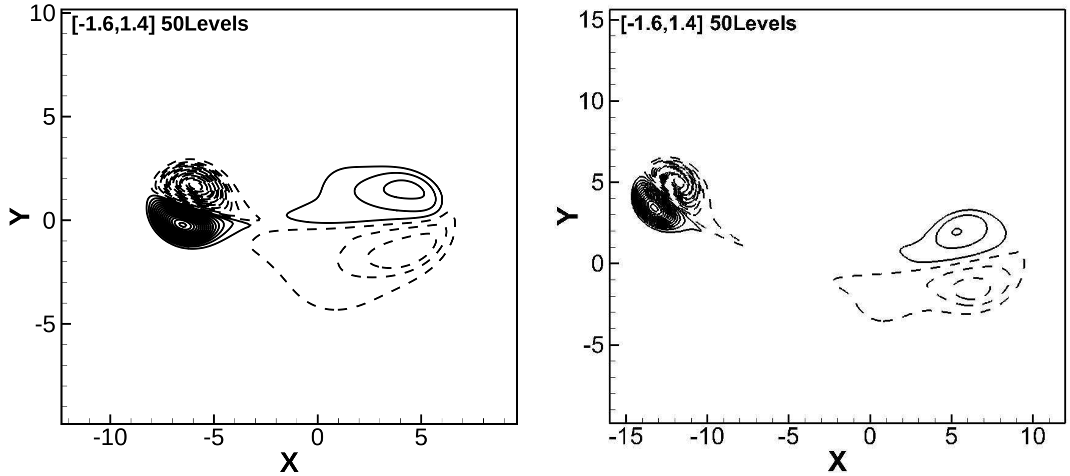

(c)$t = 60$ (d) $t = 100$

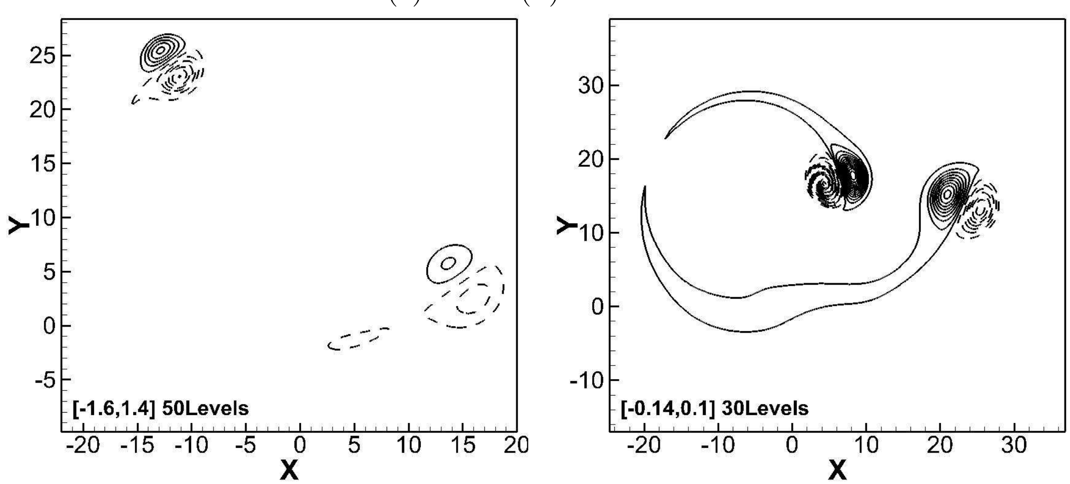

(e)$t = 300$ (f) $t = 700$

Figure 3: The evolution of the vorticity field in the interaction of two counter-rotating vortices in the case of $M_{vu} = -0.5$, $M_{vd} = 0.45$, $d = 4$ and $R_{cu} = R_{cd} = 1$.

vortices without merging. The strength of both vortices is $M_{vu} = M_{vd} = 0.5$. The initial separation distance is $d = 4$. The interaction has the following features: (1) The interaction evolves into two non-symmetric vortex structures, each of which contains three vortex cores; (2) Essentially different from the interaction of two counter-rotating vortices in the first type, three vortex cores of each vortex structure evolve from the same initial vortex, with the stronger one resulting from the inner layer of the initial vortex. The outer layer becomes a vortex strip and separates into two vortex cores around the stronger one.

Type III: The merging of two co-rotating vortices

Under certain conditions, the interaction of two co-rotating vortices will result in their merger [40], which is a key phenomenon in shear layers and wake flows. Though there are many studies on the phenomenon of vortex merging, most studies focus on the condition for two vortices to merge together [41]. In fact, the merging process plays a very important role in the generation of aeroacoustics. Figure 5 contains the evolution of the vorticity field in the merging process of two co-rotating vortices. The strength of both vortices is $M_{vu} = M_{vd} = 0.5$. The initial separation distance is $d = 2$. Preceding the merger, the cores of the two vortices move closer, and the resulting elliptical vortices evolve into a single circular vortex with two arms. In the tail region of each arm, a weaker vortex is formed from the outer layer of the original vortex. The sign of vorticity of this weaker vortex is opposite to that of the merged core. As a result, a triple polar vorticity field takes a leapfrogging motion.

Type IV: The interaction of two vortices with a large difference in their strengths or scales

This type of interaction contains two different regimes. One is the interaction of two Taylor vortices with a large difference in their strengths. The other is the interaction between two Taylor vortices with a large difference in their spatial scales.

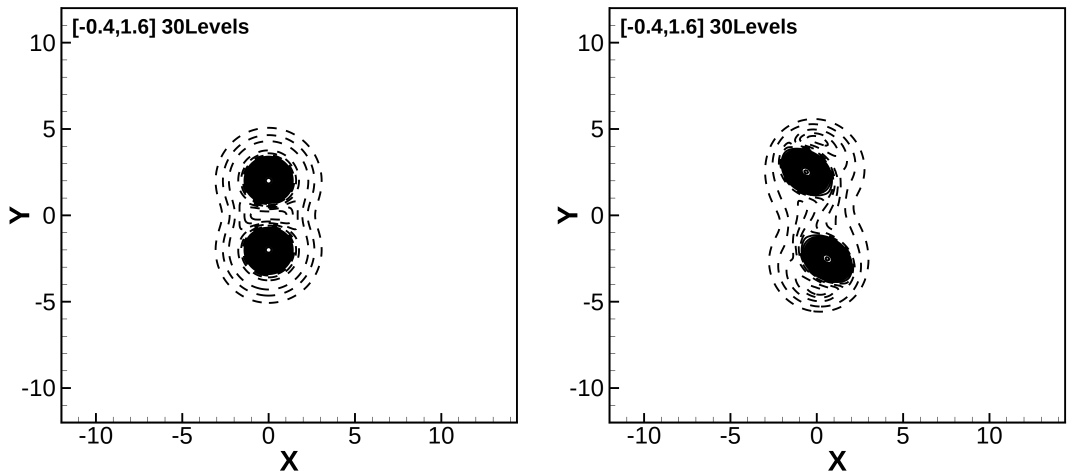

(a) $t = 0$ (b) $t = 20$

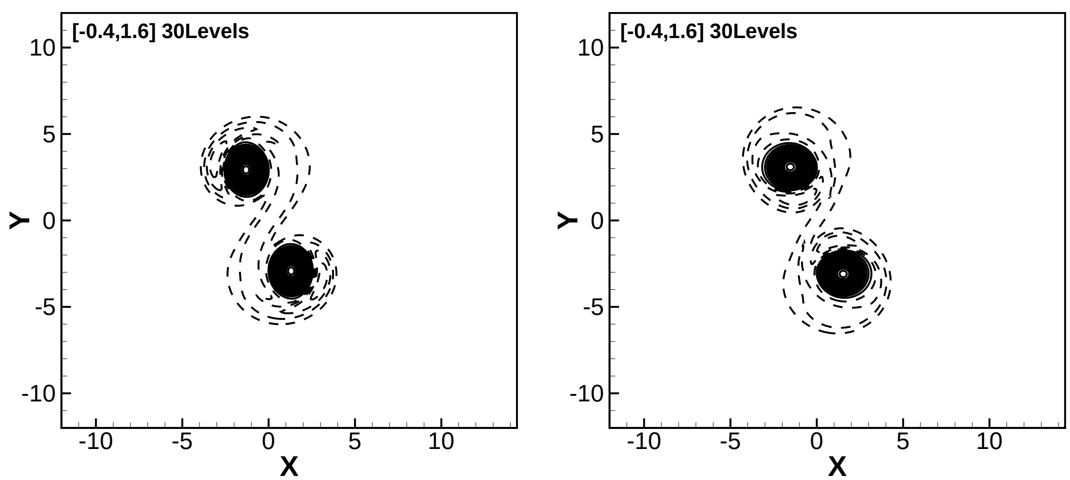

(c)$t = 40$ (d) $t = 60$

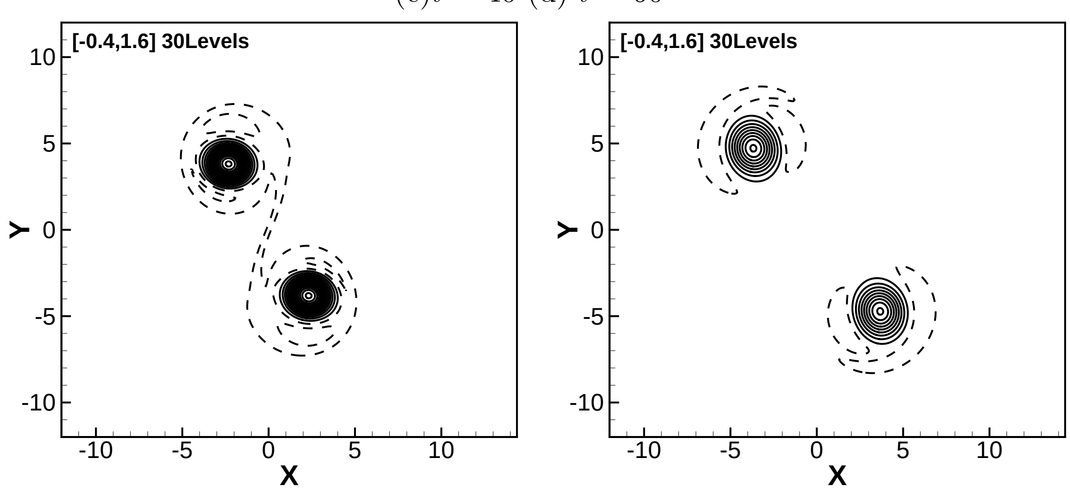

(e)$t = 100$ (f) $t = 200$

Figure 4: The evolution of the vorticity field in the interaction of two co-rotating vortices in the case of $M_{vu} = M_{vd} = 0.5$, $d = 4$ and $R_{cu} = R_{cd} = 1$.

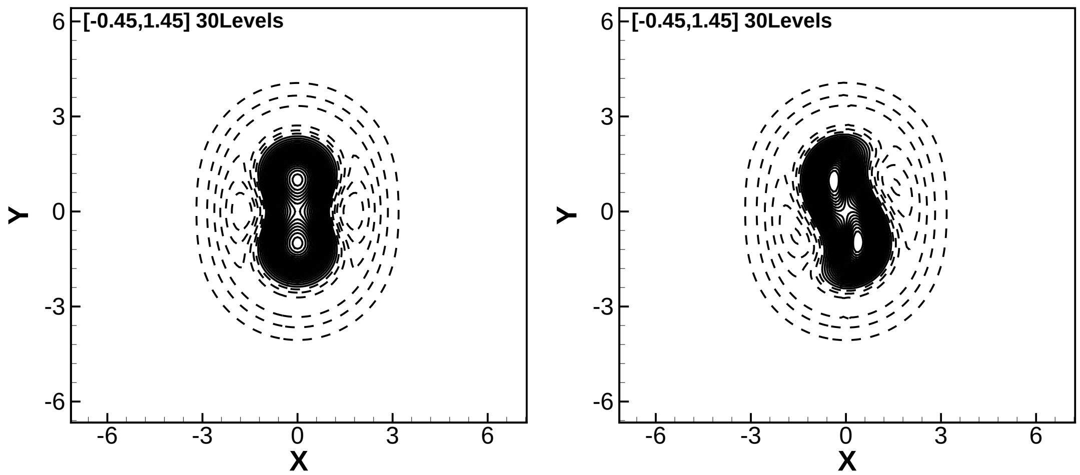

(a)$t = 0$ (b) $t = 2$

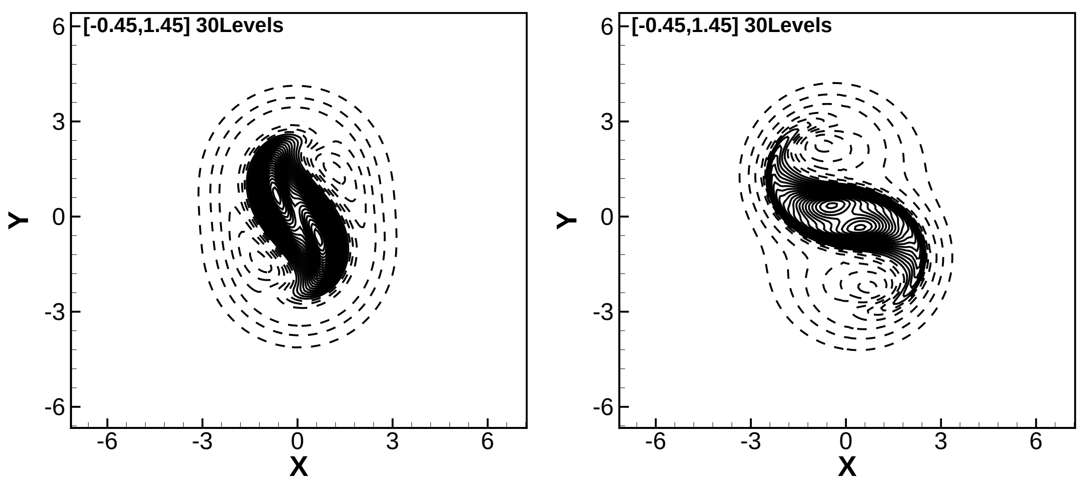

(a)$t = 4$ (b) $t = 10$

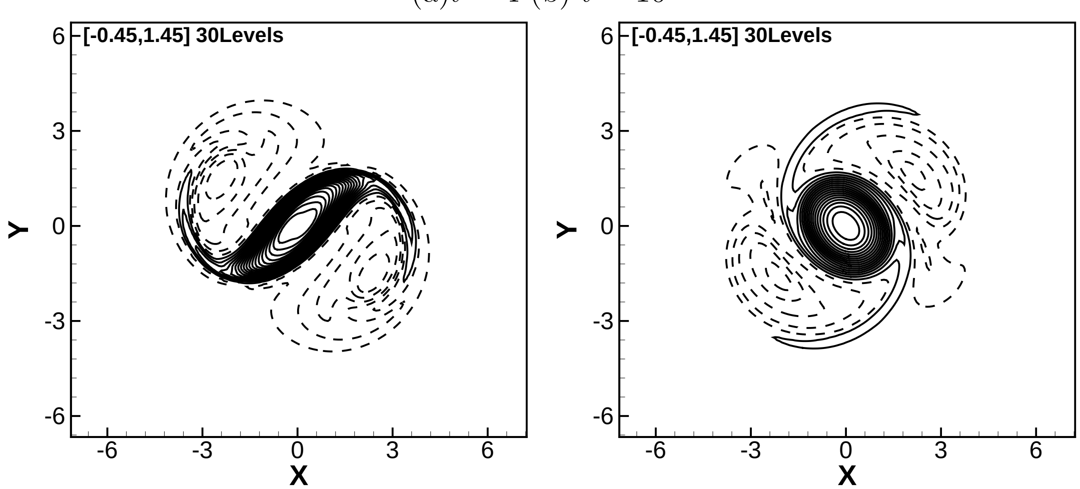

(a)$t = 20$ (b) $t = 40$

Figure 5: The evolution of the vorticity field in the merging process of two co-rotating Taylor vortices in the case of $M_{vu} = M_{vd} = 0.5$, $d = 2$ and $R_{cu} = R_{cd} = 1$.

Figure 6 contains the contours of the evolution of the vorticity field in the interaction between two counter-rotating vortices with a large difference in their strengths. The strength of the upper vortex is $M_{vu} = -0.8$ and it is $M_{vd} = 0.25$ for the lower vortex. The lower vortex is much weaker than the upper vortex. Similar to the interaction between two counter-rotating vortices of the same strength, the interaction evolves into two vortex dipoles. The cores of the two initial vortices move closer and form a stronger vortex dipole. The outer layers then separate from the initial vortices and move closer to form a weaker vortex dipole. Because there is a large difference in their strengths, both vortex dipoles are strongly non-symmetric. As a result, it seems that the weaker vortex core rotates around the stronger one quickly. At the same time, the weaker vortex dipole rotates around the stronger vortex dipole.

The same phenomenon is observed in the interaction of two co-rotating vortices with a large difference in their strengths. Figure 7 contains the evolution of the interaction between two co-rotating vortices with a large difference in their strengths. The strength of the upper vortex is $M_{vu} = 0.8$ and that of the lower vortex is $M_{vd} = 0.25$. The initial separation distance is $d = 4$. We can observe that the interaction also results in the formation of two vortex dipoles. Different from the above case, each vortex dipole comes from one of the initial vortices. The inner layer of the initial vortex forms the stronger vortex core of the vortex dipole and the outer layer forms the weaker core of the vortex dipole. The weaker vortex core rotates around the stronger one. The distance between the two vortex dipoles becomes larger during the evolution.

To study the effect of spatial scales, we study the interaction of two vortices with a large difference in their radii. Figure 8 contains the contours of the evolution of the vorticity field in the interaction between two counter-rotating vortices with a large difference in their spatial scales. The strengths of the upper and the lower vortices are the same with $M_{vu} = -0.5$ and $M_{vd} = 0.5$, while there is a large difference in the radii of the vortices. They are $R_{cu} = 1.0$ and $R_{cd} = 0.2$ respectively. As can be seen from Figure 8, we find that the smaller vortex

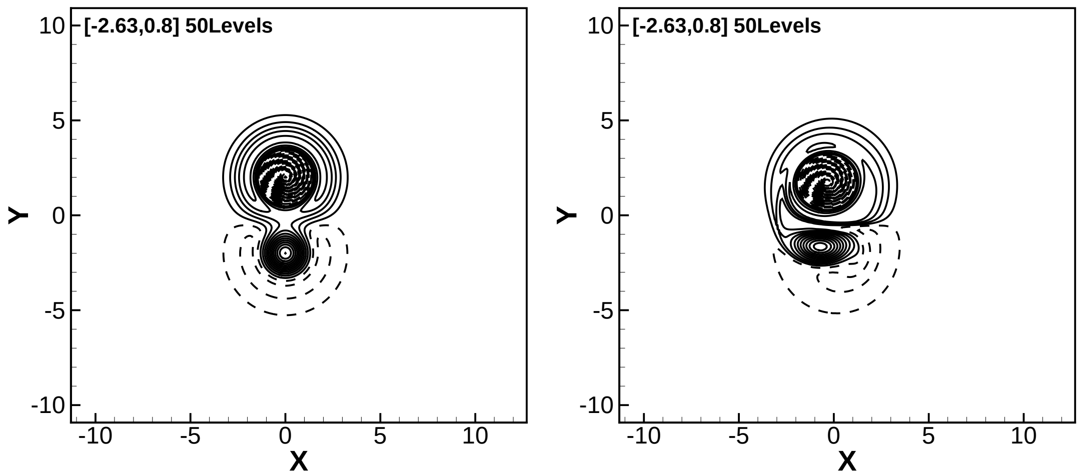

(a) $t = 0$ (b) $t = 20$

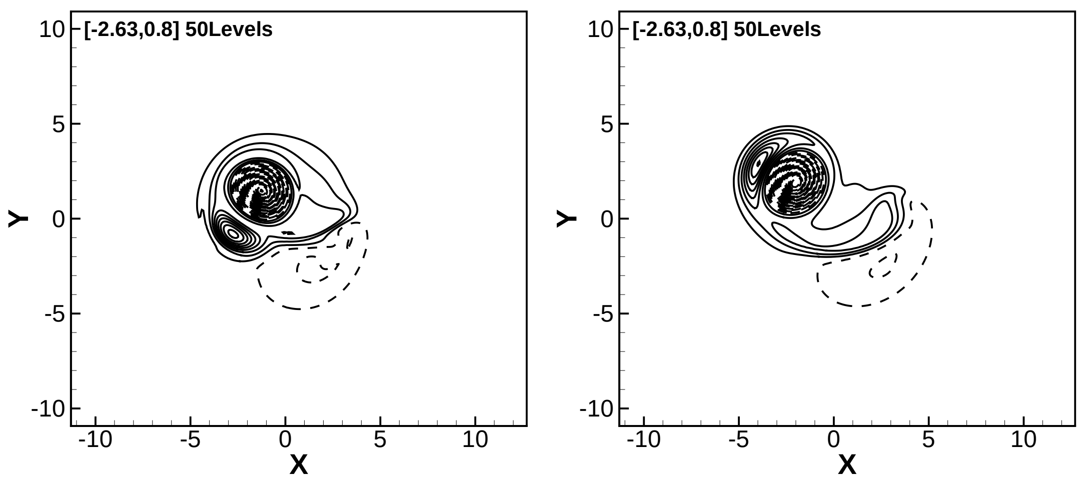

(c)$t = 40$ (d) $t = 60$

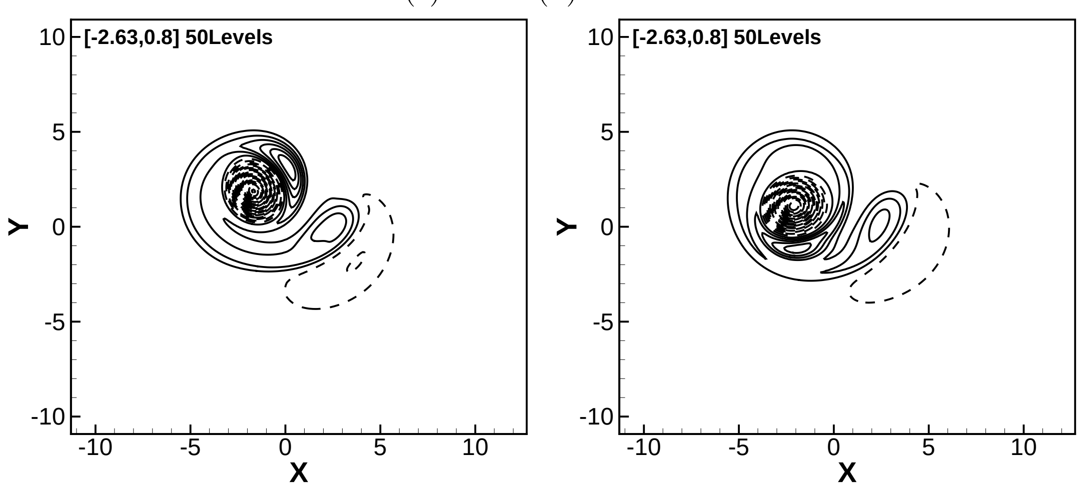

(e)$t = 80$ (f) $t = 100$

Figure 6: The evolution of the vorticity field in the interaction of two counter-rotating vortices with a large difference in their strengths in the case of $M_{vu} = -0.8$, $M_{vd} = 0.25$, $d = 4$ and $R_{cu} = R_{cd} = 1$.

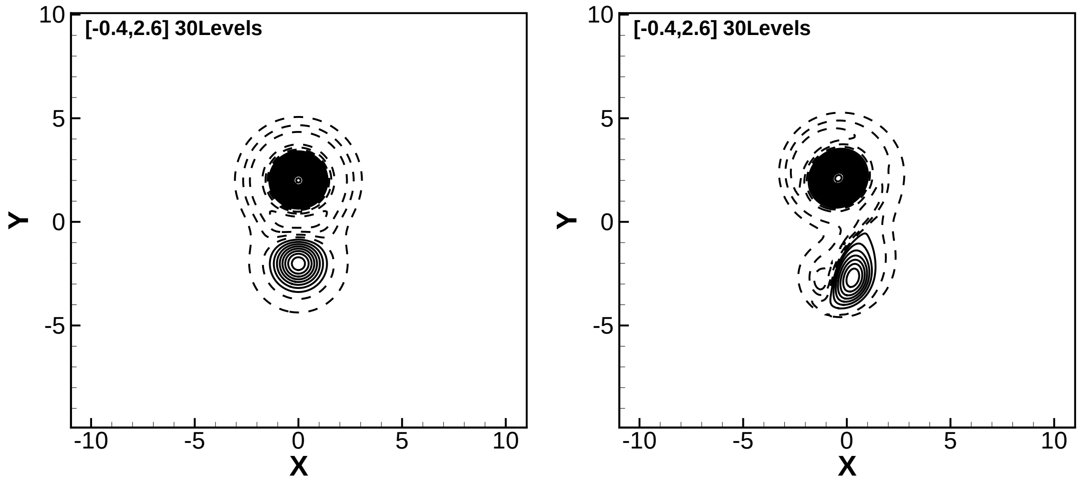

(a) $t = 0$ (b) $t = 20$

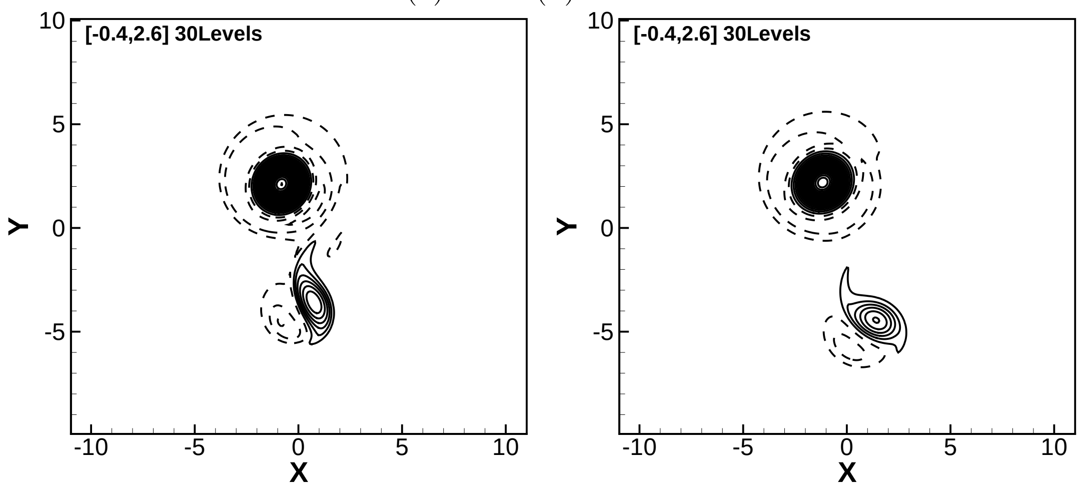

(c)$t = 40$ (d) $t = 60$

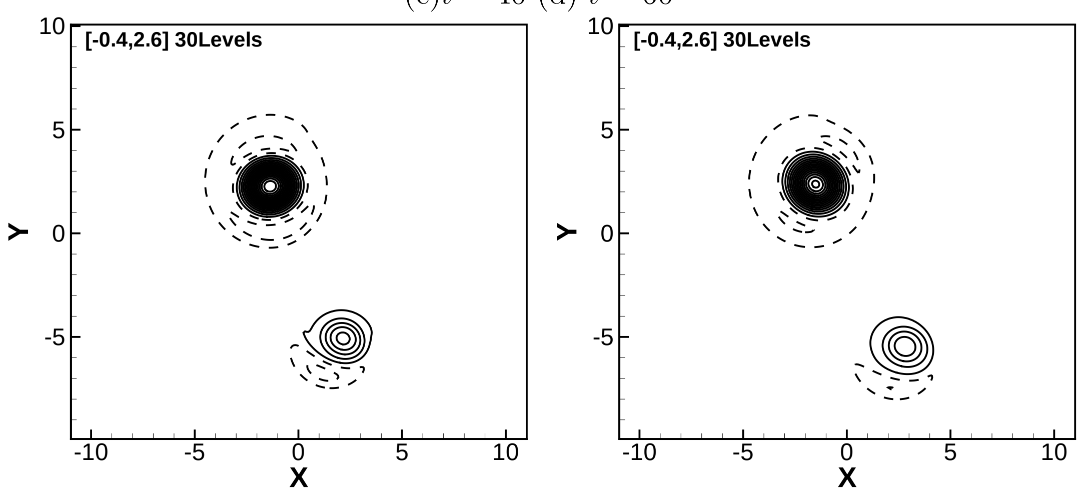

(e)$t = 80$ (f) $t = 100$

Figure 7: The evolution of the vorticity field in the interaction of two co-rotating vortices with a large difference in their strengths in the case of $M_{vu} = -0.8$, $M_{vd} = 0.25$ and $d = 4$ and $R_{cu} = R_{cd} = 1$.

goes into the outer layer of the larger vortex and rotates around the larger one. After a time period, two weaker vortices are formed around the larger one. The initial circular vortices are pressed into elliptical shapes. A triple polar vortex structure is formed. It takes a leapfrogging motion.

Comparing the interactions in these four types, we find that the first type is a basic type. Except for the merging of two co-rotating vortices in some specific conditions (which we have not attempted to determine), two vortex dipoles and triple polar vortex structures are formed. If there is a large difference in their scales, either in the strengths or in spatial scales, the vortex dipoles are strongly non-symmetric. As a result, the weaker vortex core of the dipole rotates around the stronger one continuously just like a satellite.

3.2 Sound generation in the two-dimensional interaction of two Taylor vortices

In the previous section, we have shown the dynamic feature of the two dimensional interaction of two Taylor vortices. This dynamic process can generate acoustic noise. In this section, we will explore the sound waves generated by the two-dimensional interaction and study the relationship between the sound generation and the dynamic process.

Figure 9 contains the instantaneous contours and radial distribution of far field sound pressure fluctuations $\Delta p = \frac{p-p_0}{p_0}$ at the typical time $t = 200$ for two typical cases. One is the interaction of two counter-rotating vortices in the case of $M_{vu} = -0.5$, $M_{vd} = 0.5$, $d = 4$ and $R_{cu} = R_{cd} = 1$, belonging to the first type of interaction. Another is the interaction of two co-rotating vortices in the case of $M_{vu} = 0.5$, $M_{vd} = 0.5$, $d = 4$ and $R_{cu} = R_{cd} = 1$, corresponding to the second type of interaction. The sound waves generated by these types of interaction are quite different. For the first case, there are only a few sound pulses generated, but strong noise, which is quite similar to the case of two co-rotating Gaussian vortices [18], is generated in the second case. In the other types, such as the third and fourth types of the interaction, the instantaneous contours of the sound pressure are quite similar to those in Figure 9(b). Figure 10 contains the time history of the sound pressure at a monitored point

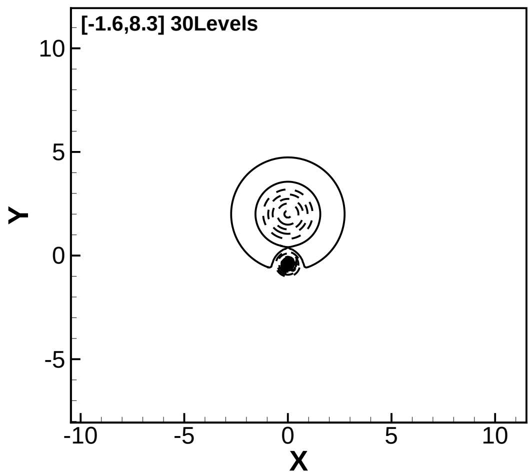

(a) $t = 0$

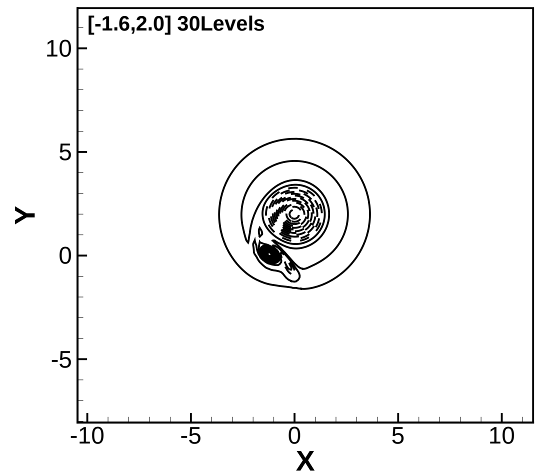

(b) $t = 10$

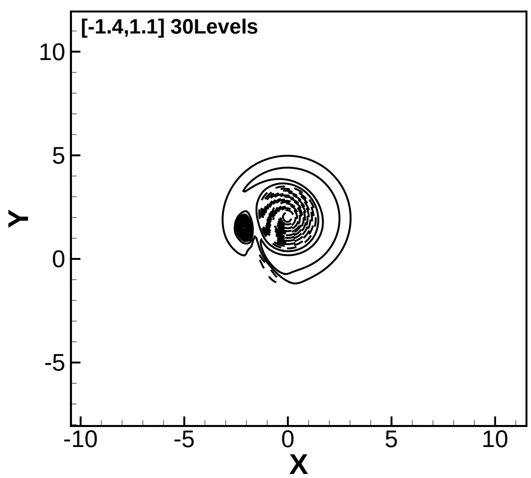

(c)$t = 20$

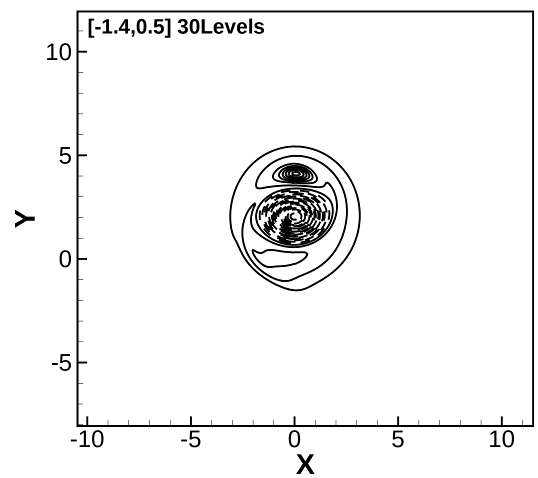

(d) $t = 40$

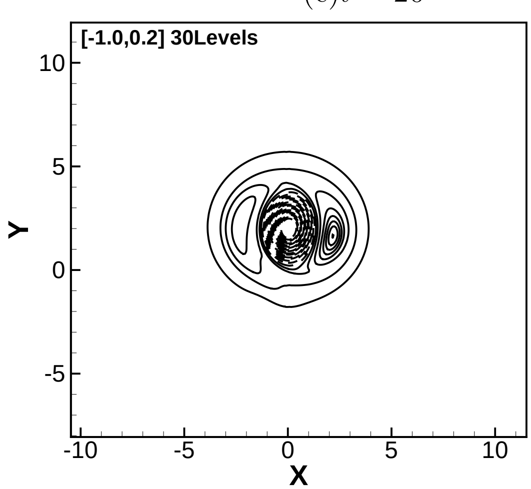

(e)$t = 60$

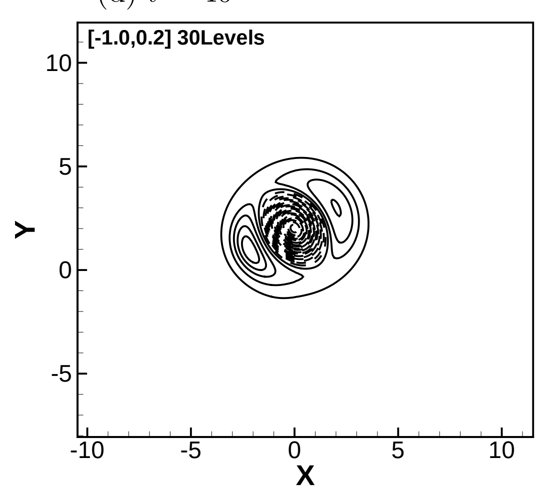

(f) $t = 100$

Figure 8: The evolution of the vorticity field in the interaction of two counter-rotating vortices with a large difference in their spatial scales in the case of $M_{vu} = -0.5$, $M_{vd} = 0.5$, $d = 2.2$, $R_{cu} = 1$ and $R_{cd} = 0.2$.

$(x, y) = (100, 0)$ for six different cases of interactions. Because the non-dimensional speed of sound wave is 1, it takes approximately a non-dimensional time $t = 100$ for the sound wave generated in the center of the vortex to propagate to the monitored point. We can observe that there are sharp sound pulses just at the setup of the interaction for all cases, which belong to the initial transient. Following the initial transient are the sound waves generated by the interaction of the two vortices. Again, we can find there are only a few sound waves generated by the first type of interaction. The noises generated by the other interactions contain two components. One is the high frequency component with a high amplitude. The other is the low frequency component with a low amplitude. Since the sound waves generated by the first type of interaction is essentially different with the other types of interaction, we discuss the mechanism of sound generation for the two types of interaction separately.

3.2.1 The mechanism of sound generation by the first type of interaction

To analyze the sound waves generated by the first type of interaction, we again plot the time history of the sound pressure at the two monitored points $(x, y) = (100, 0)$ and $(x, y) = (0, 100)$, which is shown in Figure 11. The solid line represents the time history of the sound pressure at the point $(x, y) = (100, 0)$, while the dashed line represents the sound pressure at the point $(x, y) = (0, 100)$. We can observe that the pressure fluctuations at the point $(x, y) = (0, 100)$ have the same magnitude but opposite sign to those at the point $(x, y) = (100, 0)$. To analyze the mechanism of sound generation in this interaction, we plot the instantaneous contour in Figure 12 of the Lamb vector $\nabla \bullet (\rho\omega \times u)$, which is the source term of the sound equation given by Powell [2]

$$\left(\frac{1}{c_0^2} \frac{\partial^2}{\partial t^2} - \nabla^2 \right) P' = \nabla \bullet (\rho\omega \times u). \tag{2}$$

From Figure 12, we can observe that the contours have a similar pattern with the contours of vorticity given in Figure 2. Two vortex dipoles are formed, which are advected to opposite directions by the induced velocity. The difference is that the contours of the Lamb vector have three regions. The first is the region of the vortex core. The second is the outer region

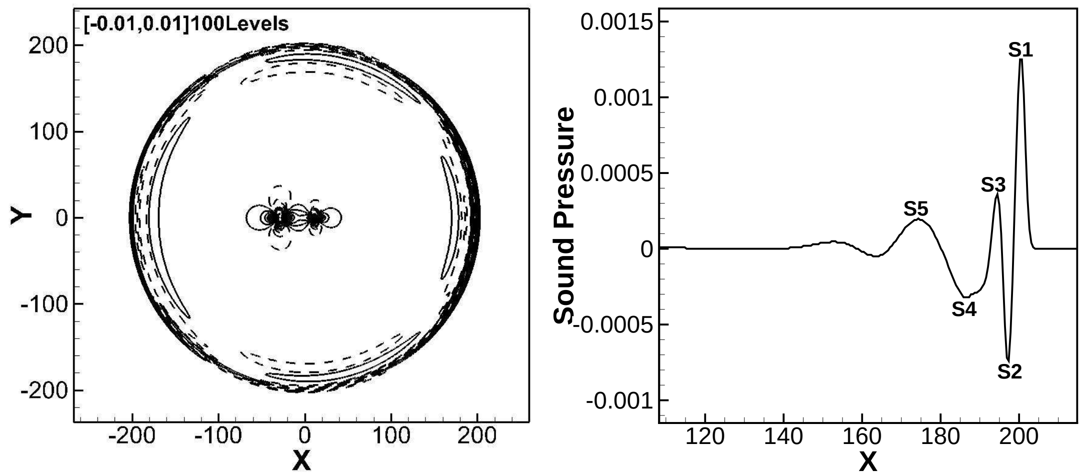

(a) Two counter-rotating vortices in the case of $M_{vu} = -0.5$, $M_{vd} = 0.5$, $d = 4$ and $R_{cu} = R_{cd} = 1$.

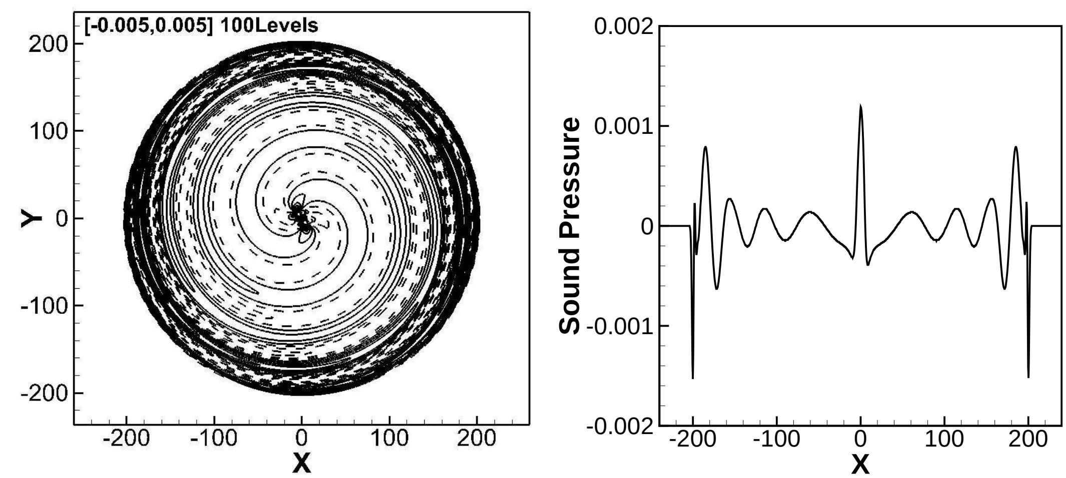

(b) Two co-rotating vortices in the case of $M_{vu} = M_{vd} = 0.5$,$d = 4$ and $R_{cu} = R_{cd} = 1$.

Figure 9: The instantaneous contours (left) and radial (middle) distributions (right) of the sound pressure $\Delta p = \frac{p-p_0}{p_0}$ at the typical time $t = 200$ in the two dimensional interaction of two Taylor vortices. Solid lines in the contours represent $\Delta p > 0$ while dashed lines represent $\Delta p < 0$.

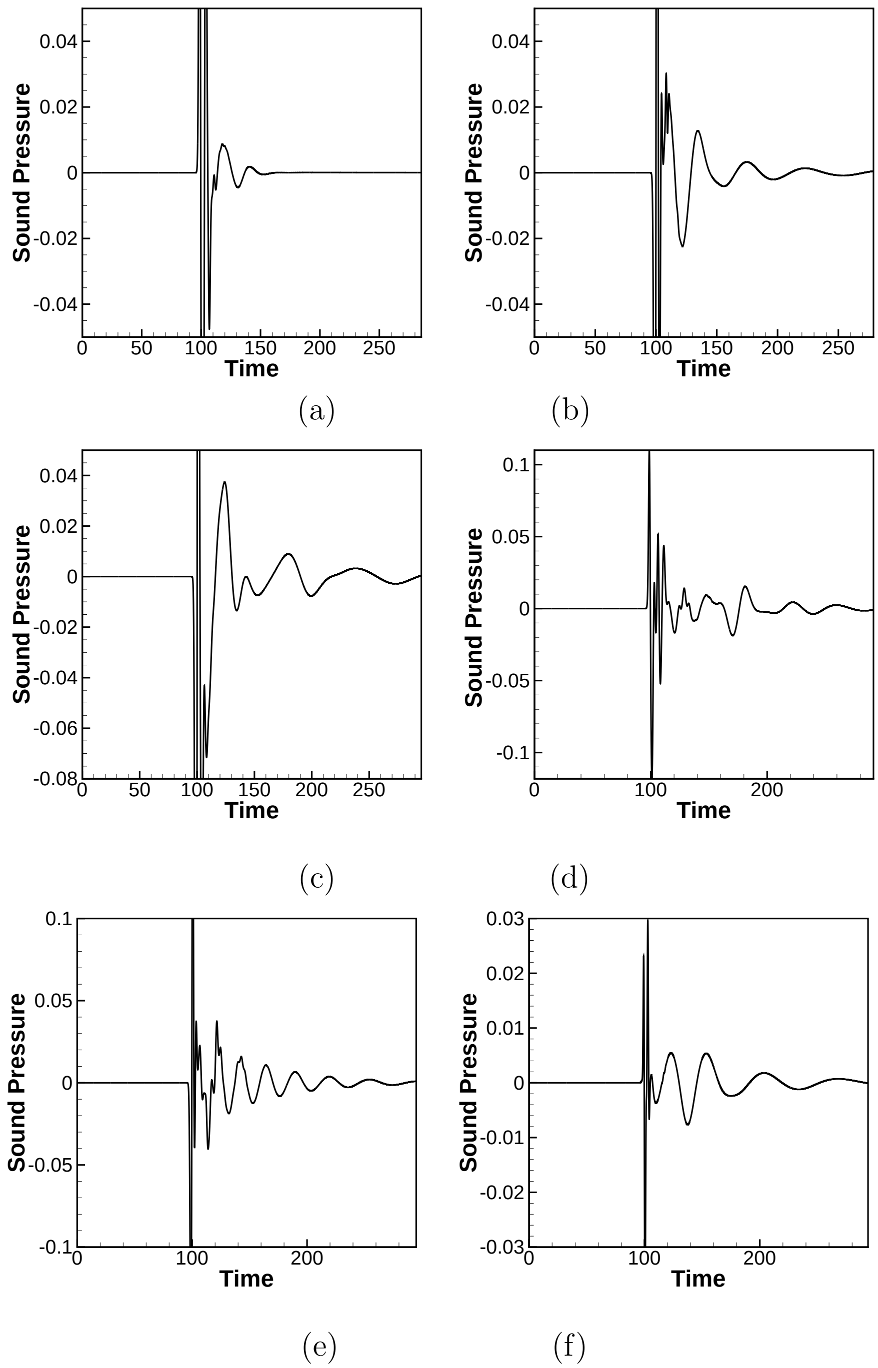

Figure 10: The time history of the sound pressure at the monitored point (100,0) in the two dimensional interaction of two Taylor vortices. (a) The interaction of two counter-rotating vortices in the case of $M_{vu} = -0.5$, $M_{vd} = 0.5$, $d = 4$ and $R_{cu} = R_{cd} = 1$. (b) The interaction of two co-rotating vortices in the case of $M_{vu} = M_{vd} = 0.5$, $d = 4$ and $R_{cu} = R_{cd} = 1$. (c) The merging of two co-rotating Taylor vortices in the case of $M_{vu} = M_{vd} = 0.5$, $d = 2$ and $R_{cu} = R_{cd} = 1$. (d) The interaction of two counter-rotating vortices with a large difference in their strengths in the case of $M_{vu} = -0.8$, $M_{vd} = 0.25$, $d = 4$ and $R_{cu} = R_{cd} = 1$.. (e) The interaction of two co-rotating vortices with a large difference in their strengths at the typical time $t = 200$ in the case of $M_{vu} = 0.8$, $M_{vd} = 0.25$, $d = 4$ and $R_{cu} = R_{cd} = 1$. (f) the interaction of two counter-rotating vortices in the case of $M_{vu} = -0.5$, $M_{vd} = 0.5$, $d = 2.2$, $R_{cu} = 1$ and $R_{cd} = 0.2$.

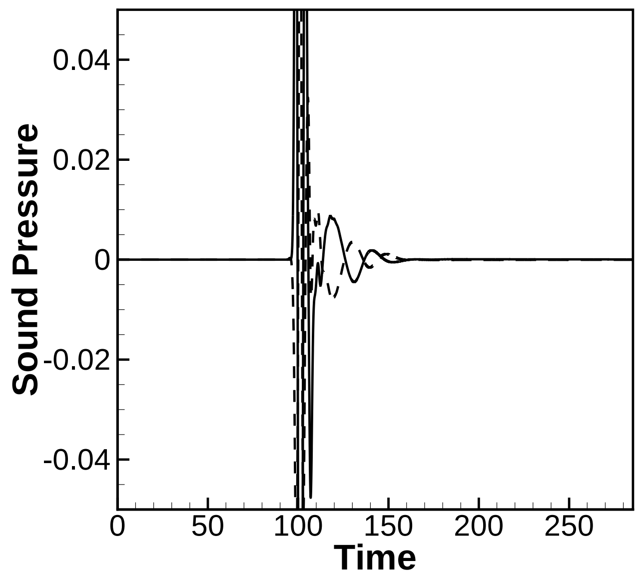

Figure 11: The time history of the sound pressure at the two monitored points (solid for (100,0) and dash for (0,100)) in the interaction of two counter-rotating vortices in the case of $M_{vu} = -0.5$, $M_{vd} = 0.5$, $d = 4.$ and $R_{cu} = R_{cd} = 1$.

of the vortex and the third is the region connecting the two vortices. Tang and Ko [24, 25] showed that the vortex sound is generated by the motion of vortex centroid and the unsteady deformation. In this interaction, the outer region of the initial vortices is stripped out from the vortex core and forms a weaker vortex dipole. The cores of the initial vortices form a stronger vortex dipole. This process finishes at approximately $t = 50$. After the vortex dipoles are formed, they are advected to opposite directions and keep moving. This belongs to the motion of the vortex centroid. The time history of the sound pressure shown in Figure 11 indicates that the sound waves are generated before $t = 50$, which means that it is generated by the process of the distortion of the initial vortices and the formation of vortex dipoles. However, after $t = 50$, there is no significant pressure fluctuation. There might be two reasons. The first might be that the sound pressure generated by the motions of two vortex dipoles is very weak compared to those generated by the formation of the vortex dipoles. The second might be that the Reynolds number is small and the viscous effect is significant.

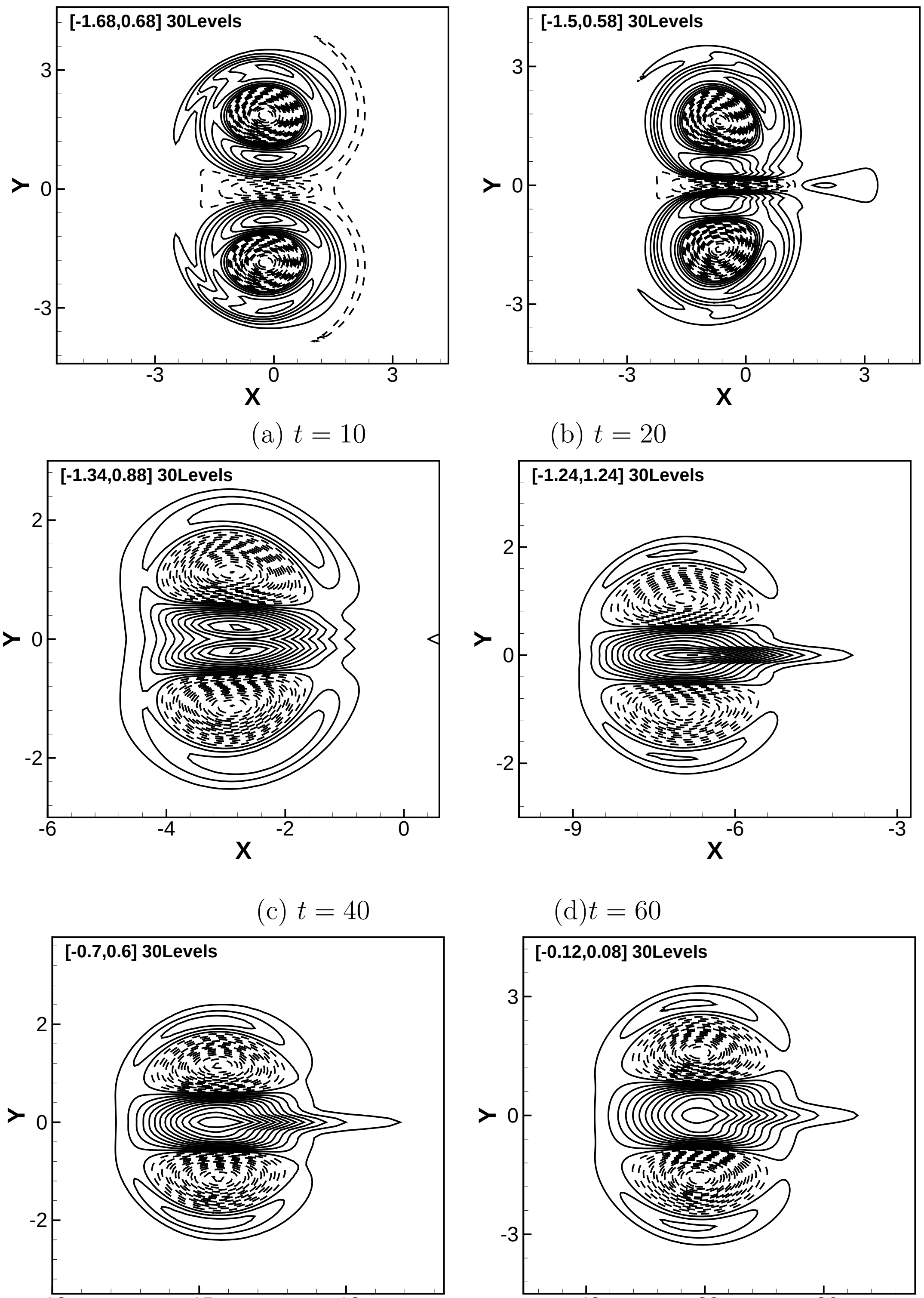

(a) $t = 10$ (b) $t = 20$

(c) $t = 40$ (d)$t = 60$

(e) $t = 100$ (f) $t = 300$

Figure 12: The evolution of the Lamb vector in the interaction of two counter-rotating vortices in the case of $M_{vu} = -0.5$, $M_{vd} = 0.5$, $d = 4$ and $R_{cu} = R_{cd} = 1$.

3.2.2 The mechanism of sound generation by the other types of interaction

The sound waves generated by the second, third and fourth types of interactions have similar patterns. Hence, we use a representative case to analyze the mechanism of sound generation. It is the interaction of two Taylor vortices with a large difference in their strengths and spatial scales.

Figure 13 contains the time history of the sound pressure at two monitored points, $(x, y) = (100, 0)$ and $(0, 100)$ in the interaction of two co-rotating vortices in the case of $M_{vu} = -0.8$, $M_{vd} = 0.25$, $d = 2.2$, $R_{cu} = 1$ and $R_{cd} = 0.2$. Again, the solid line represents the time history of the point $(x, y) = (100, 0)$ and the dashed line represents that of the point $(x, y) = (0, 100)$. They have similar magnitude but opposite sign. Before the instant $t = 140$, which corresponds to $t = 40$ of the interaction time, the sound wave has higher frequency with a large amplitude. After the instant, the sound has a decaying sinusoid feature. The frequency of the sound wave is lower and its magnitude is smaller. Figure 14 contains the time evolution of the Lamb vector (left) and vorticity (right). We can observe that both the contours of the Lamb vector and vorticity have similar patterns. The interaction has three distinguished motions. First, the initial circular vortices are distorted. The weaker vortex is teared to two vortex stripes. They interact with the stronger vortex. Second, though the position of the center of the stronger vortex does not change, the vortex core is pressed into an elliptical shape. The major axis is represented by a solid line and the minor axis is represented by a dashed line. Third, the interaction between the two vortex stripes and the core of the stronger vortex results in their leapfrogging motion. As can be seen from the time history of Figure 13, the instants of positive peaks P_1, P_2, P_3, P_4, P_5, P_6 and P_7 are 103, 121, 139, 163, 190, 223, and 262 respectively. After considering the propagation time of the sound wave from the vortex region to the monitored point, they correspond approximately to the instants that the major axis of the elliptical vortex core is located in the y-direction. While, the instants of the negative peaks M_1, M_2, M_3, M_4, M_5, M_6 and M_7 are 114, 130, 151, 176, 206, 241 and 285. They correspond approximately to the instants that

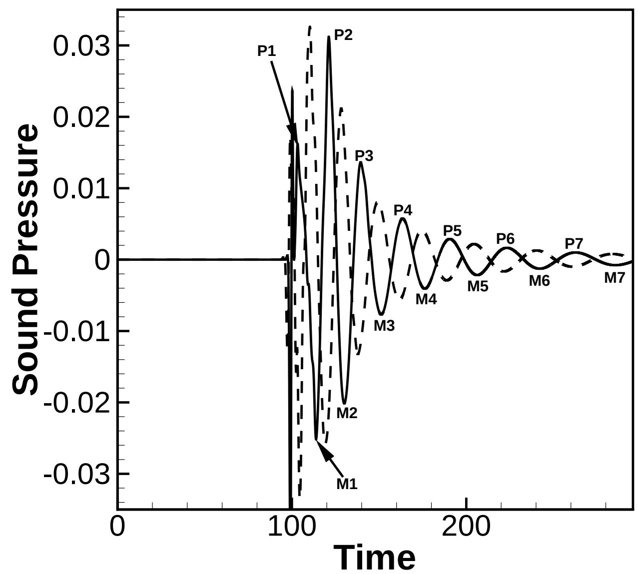

Figure 13: The time history of the sound pressure at the two monitored points (solid for (100,0) and dashed for (0,100)) in the interaction of two co-rotating vortices in the case of $M_{vu} = -0.8$, $M_{vd} = 0.25$, $d = 2.2$, $R_{cu} = 1$ and $R_{cd} = 0.2$.

the major axis is located in the x-direction. This means that the acoustic noise is generated by the leapfrogging motion, while the high frequency component is the combination of the leapfrogging and the distortion of the initial vortices.

In the case of the second type of interaction shown in the evolution of the vorticity field in Figure 4, there is the similar motion that contains the deformation of the initial vortices, the formation of the vortex stripes and the leapfrogging motion. The difference is that the vortex stripes are formed from the outer region of each vortex. There are two vorticity fields, each containing an elliptical vortex and two vortex stripes. Both of them take the leapfrogging motion which results in the generation of sound waves.

There are a lot of studies on the merging process of two co-rotating vortices [18, 27], the mechanism of sound generation in the merging process is relatively clear. However, in our case, the distribution and the structure of the initial vortices are different from those of Gaussian vortices. The merging process is different with those in [18]. Hence, the dynamic process of vortex paring and the mechanism of sound generation may be different. In Figure 15, we plot the time evolution of the Lamb vector for the third type of interaction. The

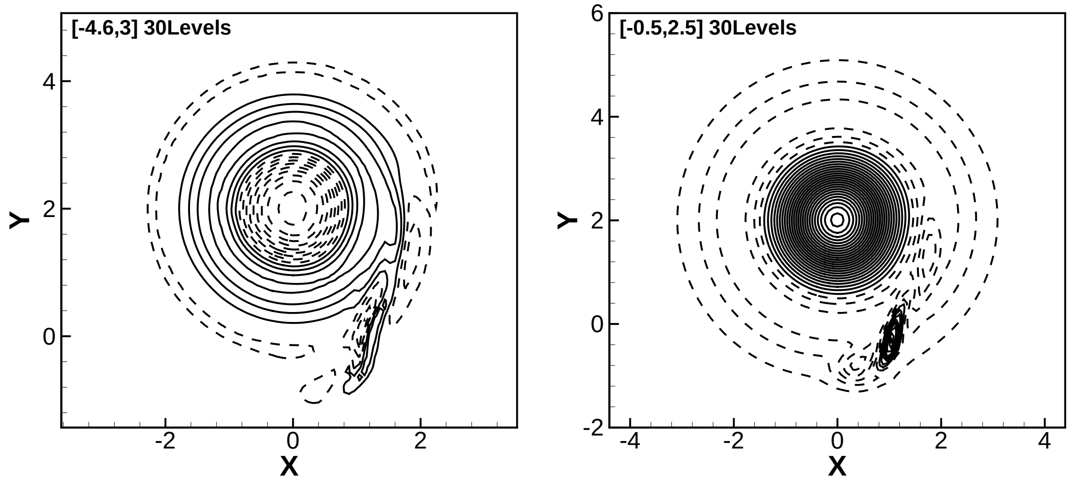

(a) $t = 6$

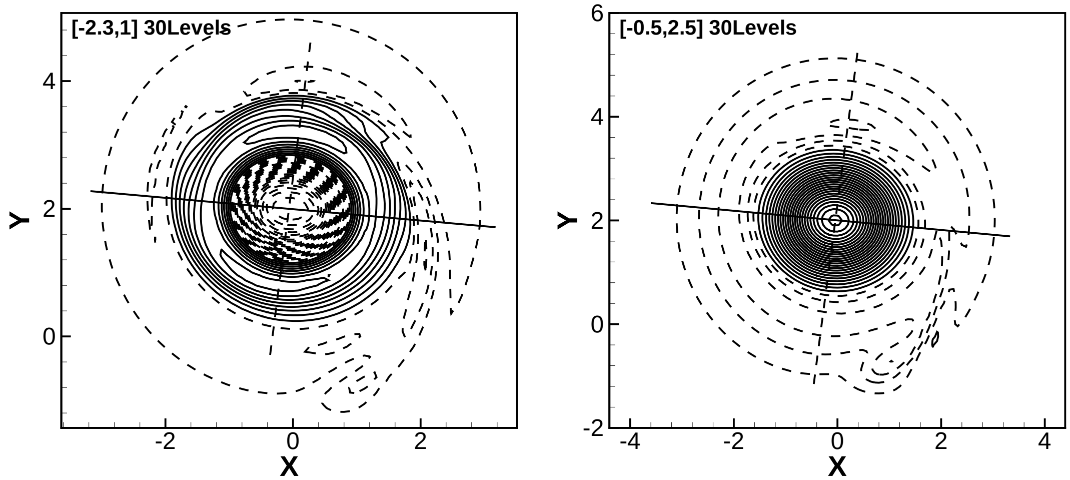

(b) $t = 14$

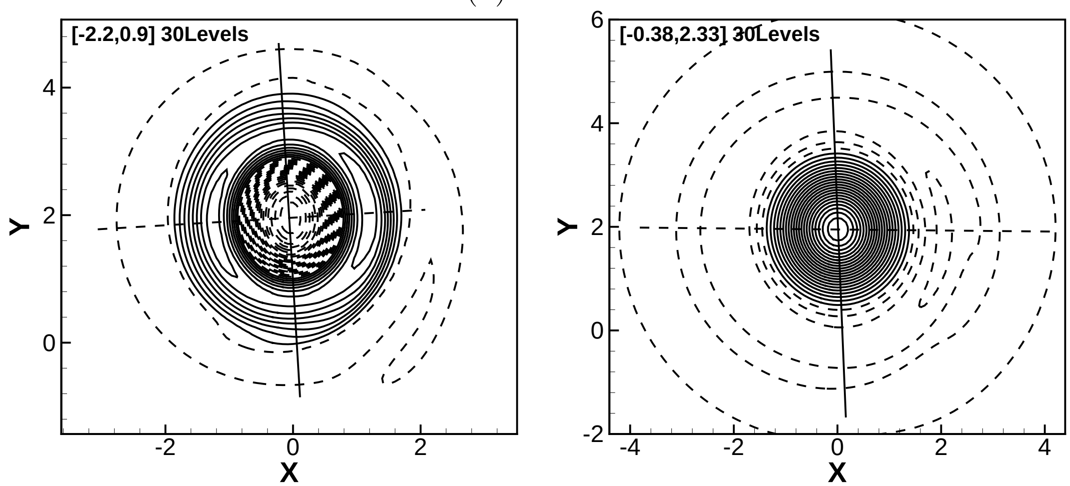

(c) $t = 24$

Figure 14: The evolution of the Lamb vector (left) and vorticity (right) in the interaction of two co-rotating vortices with a large difference in their spatial scales and strengths in the case of $M_{vu} = -0.8$, $M_{vd} = 0.25$, $d = 2.2$, $R_{cu} = 1$ and $R_{cd} = 0.2$.

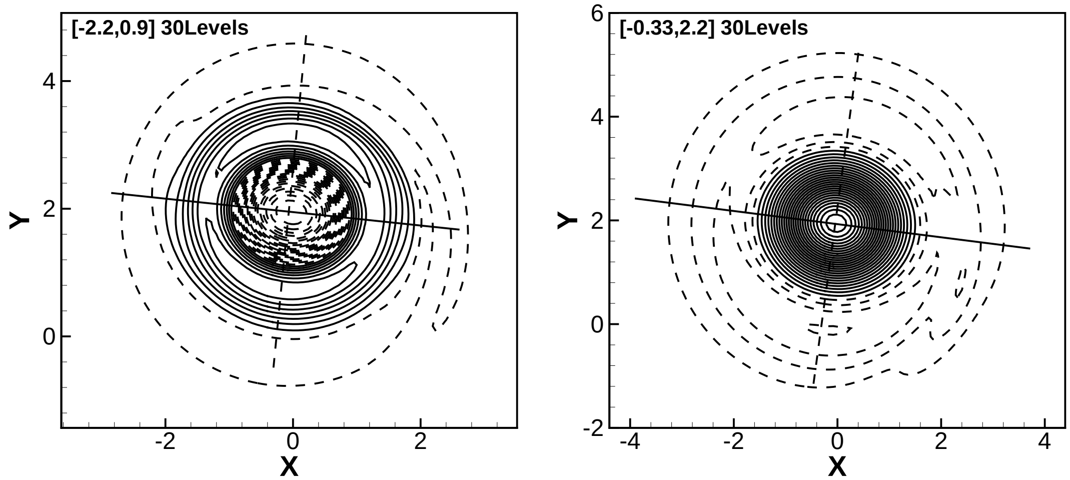

(d) $t = 32$

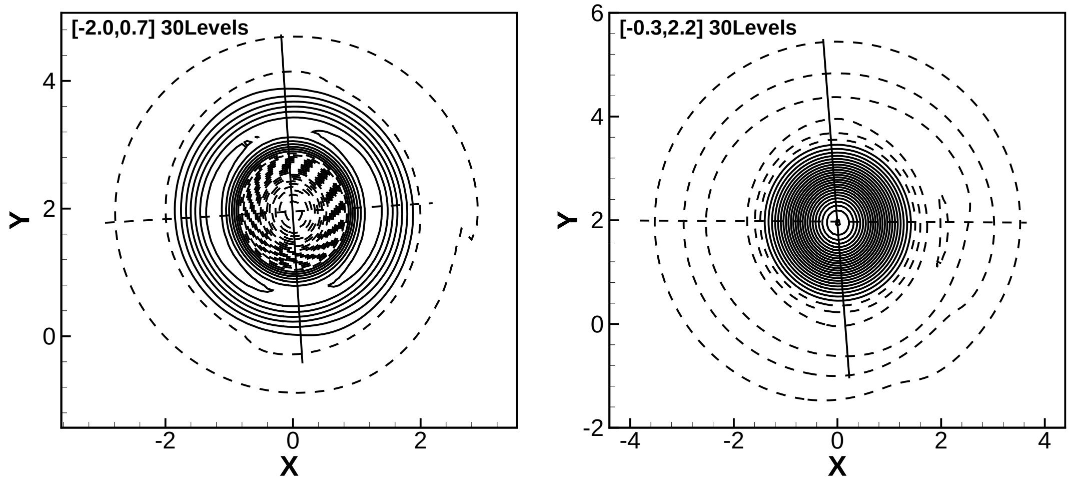

(e) $t = 44$

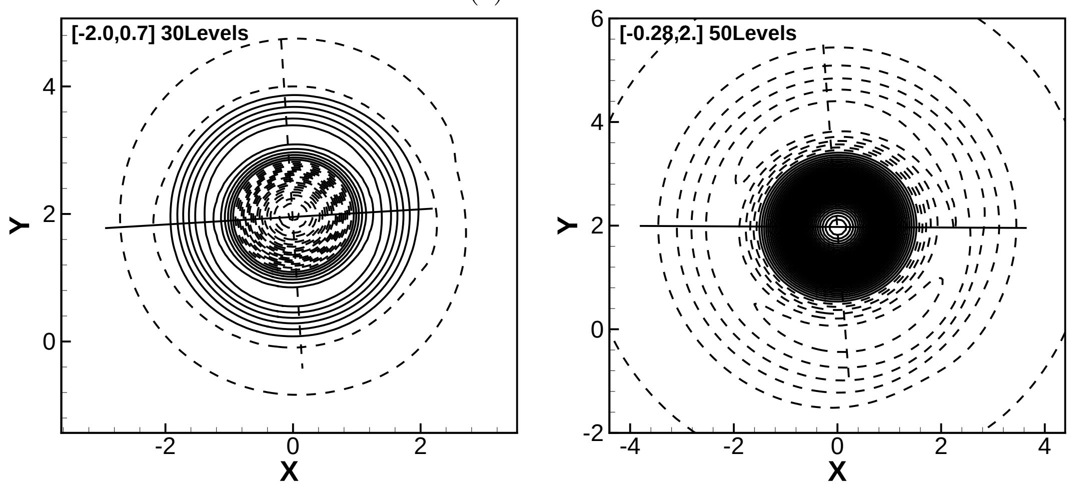

(f) $t = 56$

Figure 14: Continued.

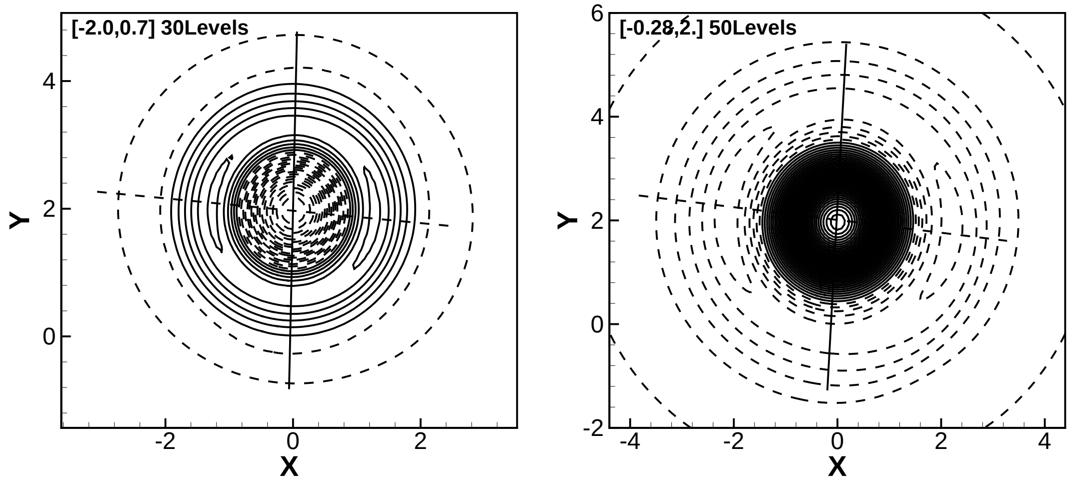

(g)$t = 66$

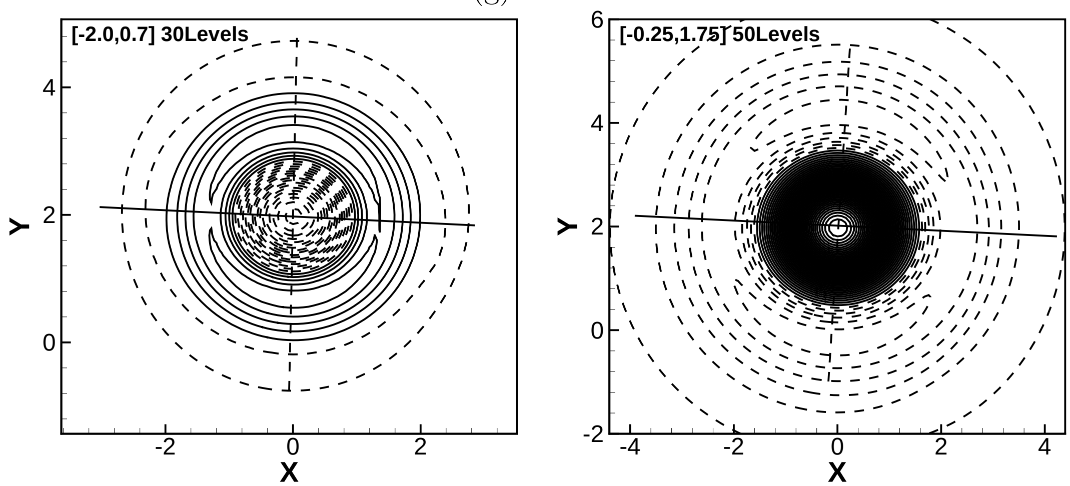

(h) $t = 80$

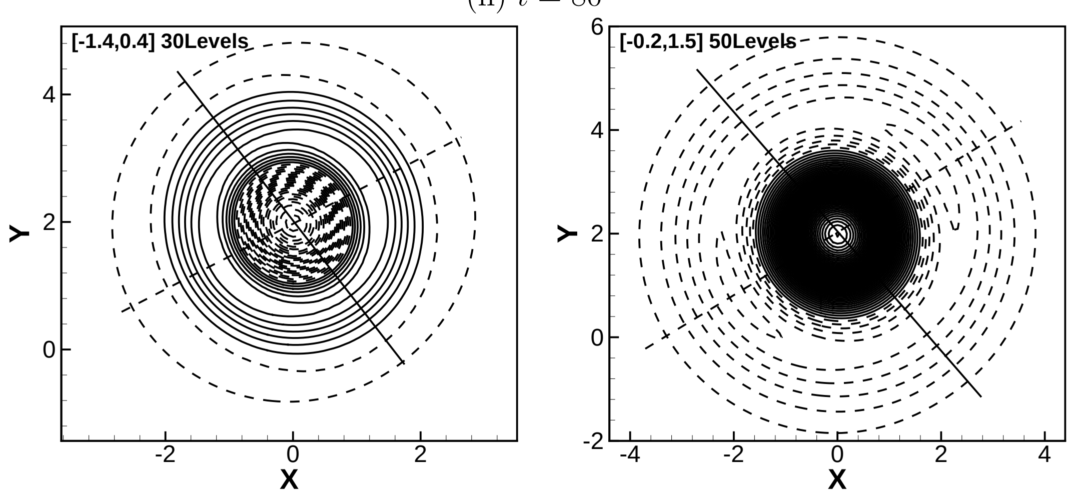

(i) $t = 100$

Figure 14: Continued.

strengths of the vortices are $M_{vu} = M_{vd} = 0.5$. The initial separation of the two vortices is $d = 2$. They are the same with those in the previous section. Compared with the time evolution of the vorticity field given in Figure 5, we can find that there are also three distinguished motions. The distortion of the initial vortices, the coalescence and the leapfrogging of three polar vortex fields. Though the separation of the initial vortices is small and vortices rotate very quickly, we can not distinguish the distortion process in this case. The structure of the initial vortices is broken. The distortion of the initial vortices is a necessary process. The coalescence is similar to that of Gaussian vortices. After the coalescence, a triple polar vortex is formed. It contains an elliptical vortex core, two weaker vortices around the vortex core and two arm-like vortex filaments. This vortex structure takes a leapfrogging motion. This dynamic process is different with that in the interaction of two Gaussian vortices [18]. The interaction of two Gaussian vortices results in the leapfrogging motion at the setup of the interaction due to the larger far field velocity and larger initial separation. After a long time leapfrogging motion, coalescence takes place and forms a single vortex. From the time history of the sound pressure at the observed point $(x, y) = (100, 0)$ in Figure 10 (c), we find that the first positive peak takes place at the instant $t = 120$, which corresponds to the instant $t = 20$ of coalescence. The following peaks correspond approximately to the instants that the connection line of the three vortex cores is in the x-direction. The minimum points, on the other hand, correspond approximately to the instants that the connection line of the three vortex centers is located in the y-direction. This means that the coalescence generates the large amplitude sound waves and the leapfrogging motion generates the low frequency sound waves with smaller amplitude. The second mechanism is similar to the mechanism of sound generation in the interaction of two vortices with a large difference in their strengths.

Because there are many vortices, eddies and structures of different scales in a turbulent flow, the interactions among these structures are very common. From the sound generated by the interactions of two Taylor vortices over all four types, we would like to emphasize the importance of the interactions among the structures with large differences in their strengths

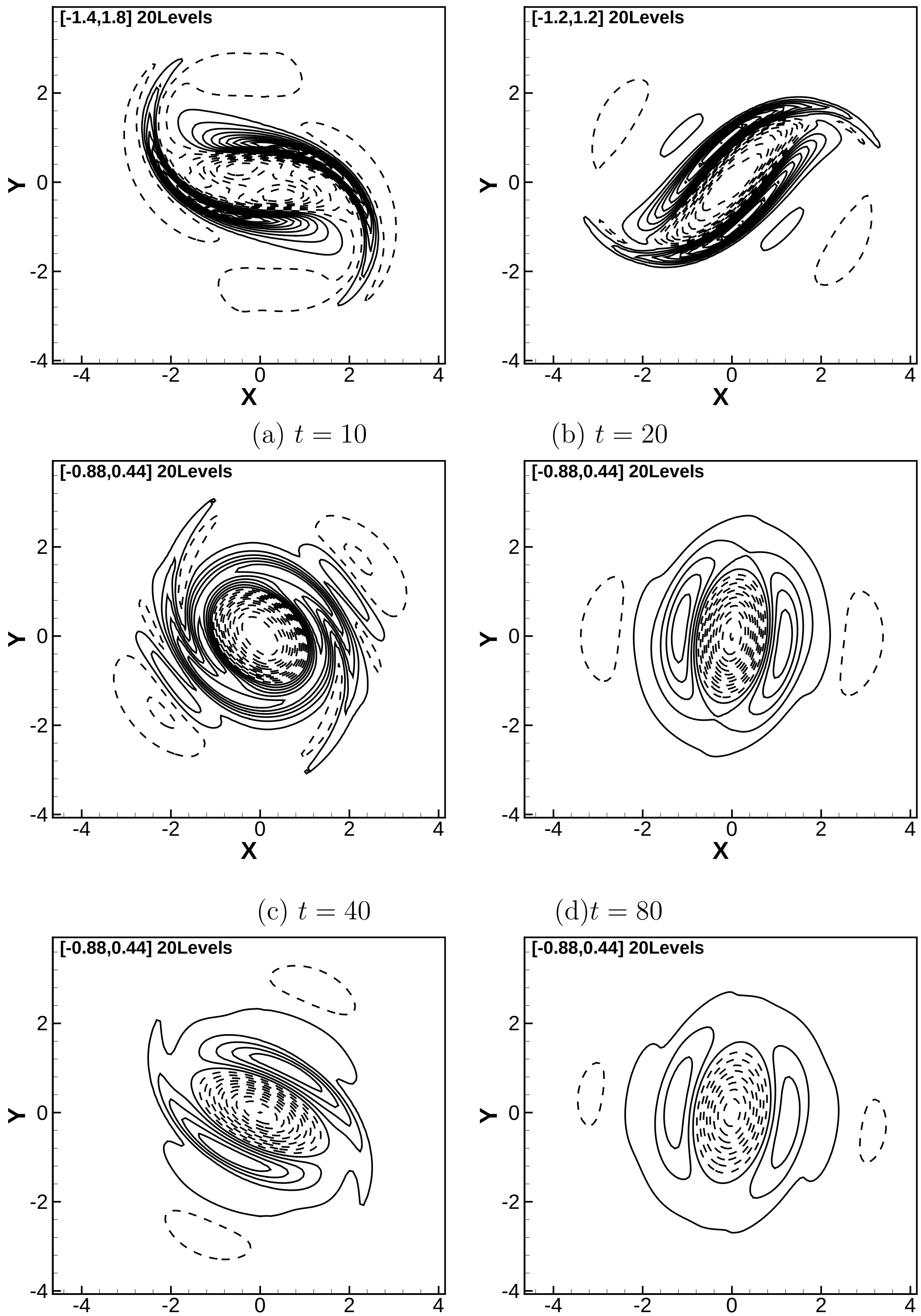

(a) $t = 10$ (b) $t = 20$

(c) $t = 40$ (d)$t = 80$

(e) $t = 100$ (f) $t = 140$

Figure 15: The evolution of the Lamb vector in the merging process of two co-rotating vortices in the case of $M_{vu} = M_{vd} = 0.5$, $d = 2$ and $R_{cu} = R_{cd} = 1$.

or scales as a key source of turbulent noise.

4 Revisit the interaction of two co-rotating Gaussian vortices

Like Taylor vortex, Gaussian vortex is also a typical vortex. There are a lot of studies [18, 42, 43] on the sound generation by the merging of two co-rotating Gaussian vortices. In this Section, we revisit the merging of two co-rotating Gaussian vortices to show the difference of sound generation with the different initial distribution and different structure.

4.1 Revisit the interaction of two co-rotating Gaussian vortices

The initial condition of the Gaussian vortex is the same as that in the papers [18, 42, 43]. The initial distribution of tangential velocity of each Gaussian vortex is given by

$$u_\theta = \frac{\Gamma}{2\pi r}(1 - e^{-\alpha r^2/R_c^2}) \tag{3}$$

with $\alpha = 1.256431$. The initial distribution of the pressure field is obtained by solving a Poisson equation with a convergence condition $\epsilon = 10^{-12}$. Unlike Taylor vortex in the previous section, all quantities are scaled by the initial half spacing between the vortices and the speed of sound a_∞ of the free stream. For comparison, all quantities including the strengths of Gaussian vortices, the initial separation distance and Reynolds number are the same with those in [18, 42, 43].

Figure 16 is the evolution of the vorticity field of the interaction of two Gaussian vortices. It is clear that coalescence takes place after a long time of leapfrogging motion. Figure 17 is the time history of dilatation at the point $(x, y) = (0, 1.2)$ and the comparison with that of Eldredge et al [43]. It is obvious that the comparison is satisfactory. Figure 18 contains the time history of separation distance of two co-rotating Gaussian vortices. It indicates that two co-rotating Gaussian vortices merges at the instant $t = 500$, which is the same with that of Eldredge et al [43], but different with that given by Mitchell et al [18].

Figure 19 is the third time derivative of the source terms

$$
\begin{aligned}
Q_1 &= 2\int\int xy\omega dxdy \\
Q_2 &= \int\int (y^2 - x^2)\omega dxdy
\end{aligned}
\tag{4}
$$

in Möhring's equation [26] to predict the far-field pressure fluctuation given by the equation

$$
P'(x,t) = \frac{\rho_0}{8\pi a_\infty^2}\int_0^\infty [\dddot{Q}_1(t^*)cos(2\theta) + \dddot{Q}_2(t^*)sin(2\theta)]d\xi \tag{5}
$$

where $t^* = t - \frac{r}{c_0}cosh(\xi)$, and θ is measured with respect to the x axis. Figure 20 contains the far-field pressure fluctuation and its comparison with that given by equation (5). Our numerical result agrees with that given by Eldredge et. al [43]. However, because of the difference in the merging instant, it is different with that given by Mitchell et al [18].

4.2 Discussion on the differences between Gaussian vortex and Taylor vortex and their effect on the sound generation

There are two main differences between Gaussian vortex and Taylor vortex. (1) The decay (with respect to r) towards free-stream flow of the physical variables such as tangential velocity, vorticity, pressure and density is much faster for a Taylor vortex than for a Gaussian vortex. For example, the tangential velocity of Taylor vortex becomes 0.00225 and 0.0000307 at the position of $\frac{r}{R_c} = 4$ and 5 respectively, while they are 0.349 and 0.280 for the Gaussian vortex. Even at a very far position to the vortex center such as $\frac{r}{R_c} = 20$, the tangential velocity for the Gaussian vortex is still 0.0699. Thus, the effective influence region of a Gaussian vortex is much larger than that of the Taylor vortex. This can be observed in Figure 21 for the comparison of the tangential velocity distribution between Gaussian and Taylor vortices. This fact leads to a great decrease for the transient effect during vortex-vortex interactions for the Taylor vortices compared with the Gaussian vortices. The large velocity in the far field of the Gaussian vortex may be the main reason of the slow and long time leapfrogging motion in the setup of the interaction between two Gaussian vortices with large initial separation. It is easier for the Taylor vortices to distinguish the different

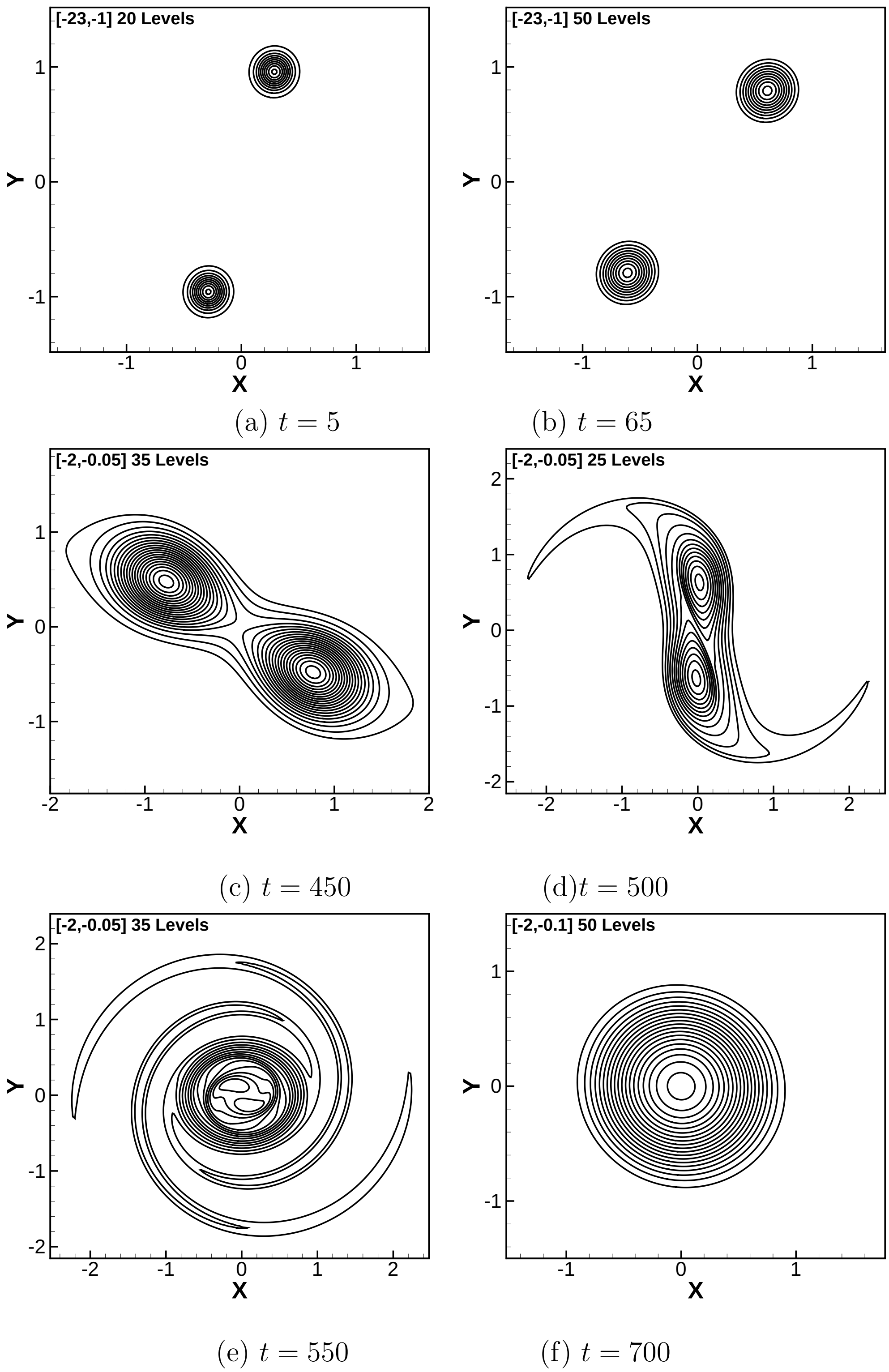

(a) $t = 5$ (b) $t = 65$

(c) $t = 450$ (d)$t = 500$

(e) $t = 550$ (f) $t = 700$

Figure 16: The evolution of the vorticity field in the interaction of two co-rotating Gaussian vortices.

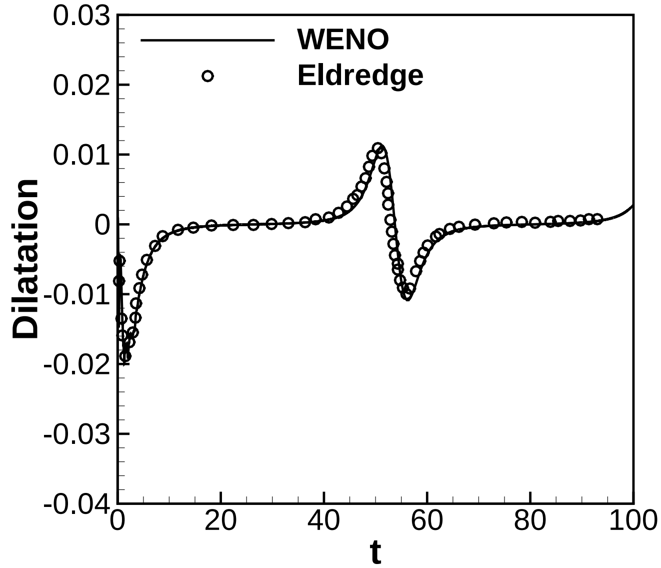

Figure 17: The time history of dilation at the point $(x, y) = (0., 1.2)$ and its comparison with that of Eldredge et al [43].

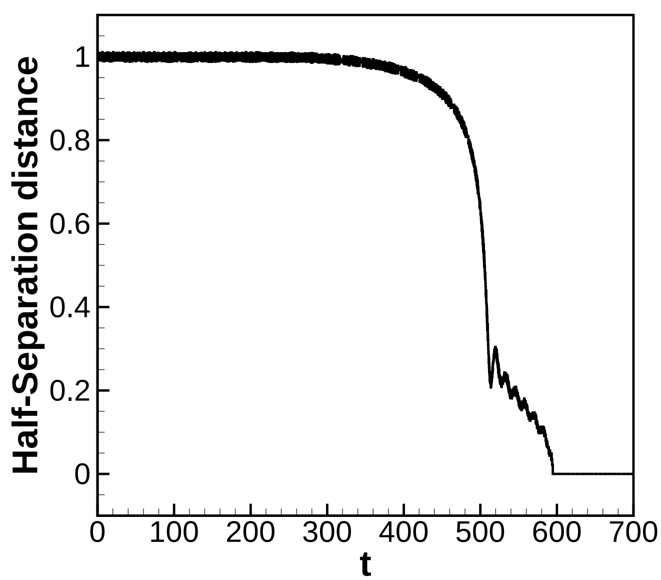

Figure 18: The time history of separation distance of two co-rotating Gaussian vortices.

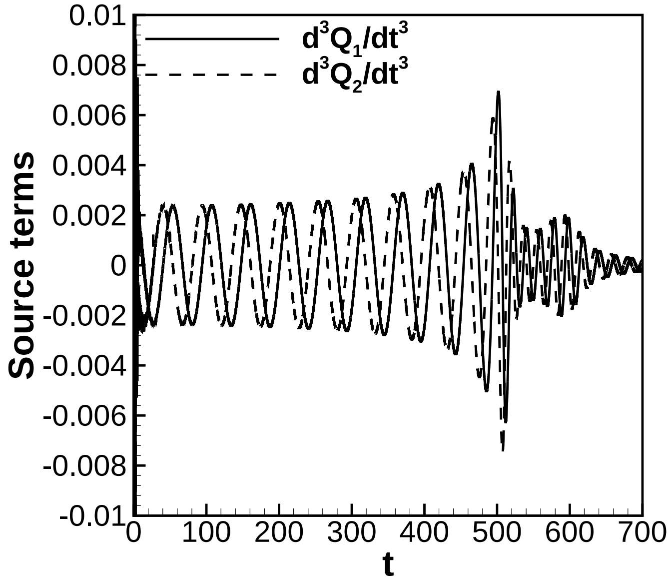

Figure 19: The time evolution of second-order moments of vorticity $\dddot{Q}_1$ and $\dddot{Q}_2$ defined by equation (4).

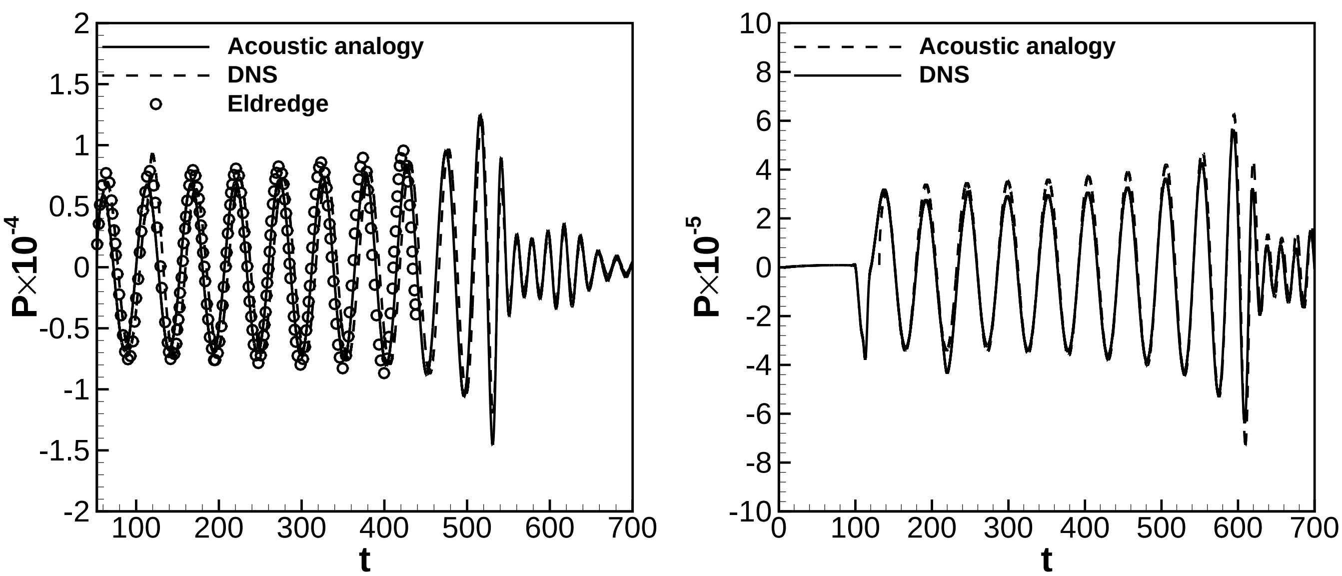

Figure 20: Far-field pressure traces at $\frac{r}{\lambda} = \frac{1}{2}$ (left) and $\frac{r}{\lambda} = 2$ (right) and the comparison between our direct numerical simulation (DNS) and that by the Möhring's equation (5).

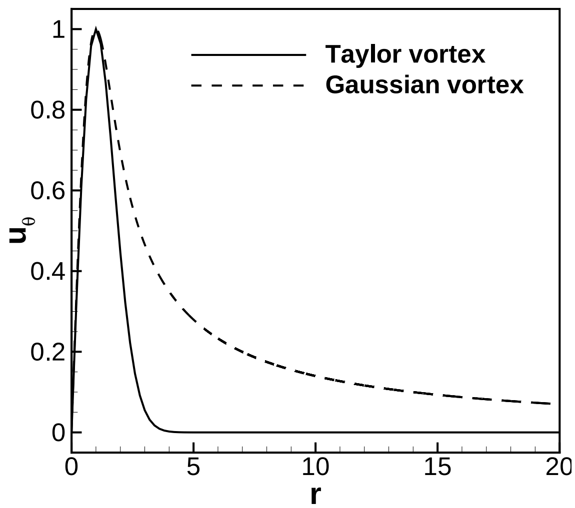

Figure 21: The comparison for the distribution of tangential velocity along radius between Taylor vortex and Gaussian vortex.

mechanism of sound generation in different dynamic processes. (2) The vortex structure is different. There are two different layers in a Taylor vortex. The vorticity has different signs in these two layers. In comparison, there is only one layer in the Gaussian vortex. Figure 22 contains the comparison of vorticity between these two different vortices. The interaction of two Taylor vortices results in the separation of these two layers and the formation of more complex vortex structures than that of the Gaussian vortices. The difference between the initial structures of the two types of vortices results the different mechanism of sound generation.

5 Discussion on the interaction of two vortices in a complex flow

Vortex is a basic element of fluid. The interaction between two or among more vortices is very common. In this section, we are interested in the decaying two-dimensional homogeneous isotropic turbulence which has a close relationship to the interaction of two vortices. The purpose of this section is to show that the the vortex-vortex interactions studied in the previous section do actually take place in two-dimensional turbulence.

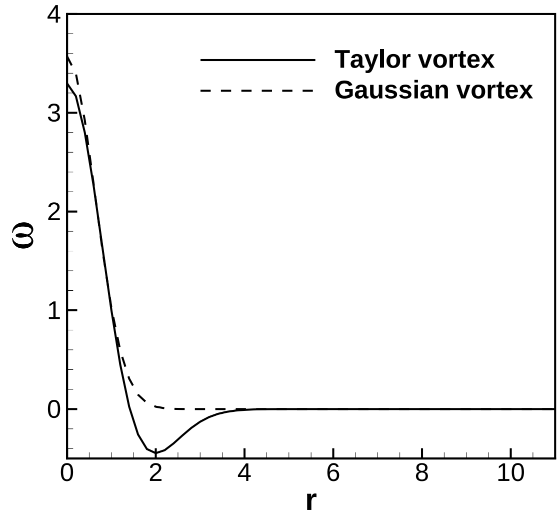

Figure 22: The comparison for the distribution of vorticity along the radius between Taylor vortex and Gaussian vortex.

Two-dimensional homogeneous decaying turbulence is an incompressible flow problem in which the kinetic energy decays. Due to the inverse energy cascade in two-dimensional turbulence, it has been receiving a lot of studies [44, 45, 46, 47].

The computational domain is a square with length 2π. Periodic boundary conditions are applied. The initial energy spectrum in the Fourier space is given by [44]

$$E(k) = \frac{a_s}{2}\frac{1}{k_p}\left(\frac{k}{k_p}\right)^{2s+1} \exp\left[-\left(s+\frac{1}{2}\right)\left(\frac{k}{k_p}\right)^2\right]$$

where $k = |k| = \sqrt{{k_x}^2 + {k_y}^2}$, $k_p = 12$ and $a_s = \frac{(2s+1)^{s+1}}{2^s s!}$. The initial flow field contains many vortices. The problem of the free decay of two-dimensional turbulence is to determine how abundant populations of vortices freely evolve with time. In this study, we solve this problem to examine the types of interaction of two vortices given in Section 3. The Reynolds number is chosen as 1000. After the study of grid convergence to confirm sufficient grid resolution, we use an uniform mesh with the grid density of 2048×2048 to simulate the two-dimensional decaying turbulence.

Figure 23 contains the time evolution of the two-dimensional decaying turbulence at typical times. The details for the turbulent characteristics can be found in [44, 45, 46, 47]. Here, we are only interested in the types of the interaction of two vortices. In Figure 23, there are three boxed regions, which represent the starting time of different types of vortex interaction. The boxed region in Figure 23(b) is the starting time of an interaction of two vortices in opposite signs of vorticity. Figure 24 contains the evolution of this interaction. We can clearly observe the formation and the evolution of a vortex dipole. The boxed region in Figure 23(a) is the starting time of an interaction of two vortices in the same sign of vorticity. Figure 25 contains the process of vortex merging. It is clear that during the interaction the two co-rotating vortices merge together to form a single vortex. Vortex merging is a dominating phenomenon for two dimensional turbulence, which is the mechanism of the inverse cascade energy [47]. The boxed region in Figure 23(c) is the starting time of an interaction of two vortices with a large difference in their scales. The time evolution of this interaction is shown in Figure 26. We can clearly observe that the smaller vortex rotates around the bigger one.

6 Concluding remarks

The two-dimensional interaction between two Taylor vortices is simulated systematically through solving the two-dimensional, unsteady compressible Navier-Stokes equations using a fifth order weighted essentially nonoscillatory finite difference scheme. The mechanism of sound generation is analyzed.

Based on an extensive parameter study on the evolution of vorticity, the two-dimensional interaction between two Taylor vortices is classified into four types. They are the interaction between two counter-rotating vortices with similar strength, the interaction between two co-rotating vortices without merging, the merging of two co-rotating vortices and the interaction of two Taylor vortices with a large difference in their strengths or scales.

The Taylor vortex considered in this paper has two layers, inner layer and outer layer. The sign of vorticity is opposite in the inner layer and the outer layer. After the distortion of the initial vortices at the setup of the interaction, new complex vorticity field is formed.

In the interaction of two counter-rotating vortices with similar strengths, two vortex

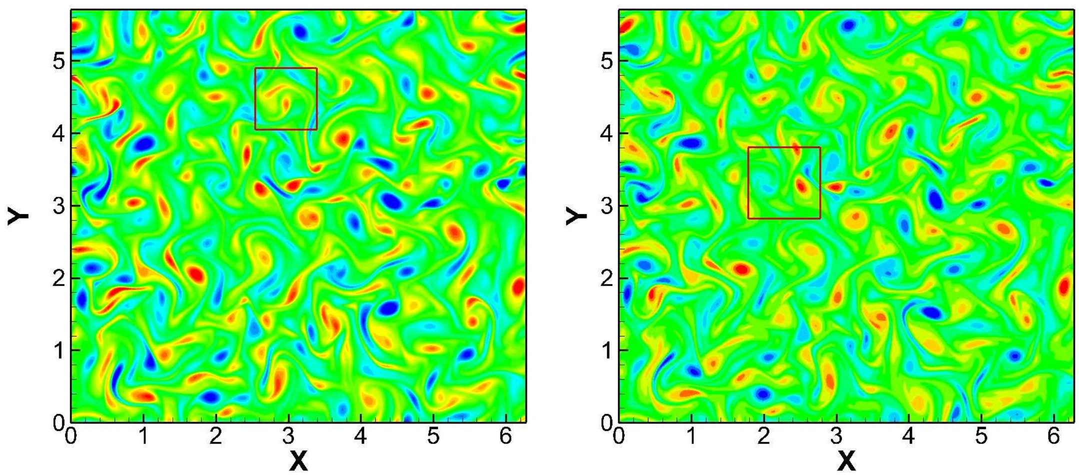

(a) $t = 0.85$,$[-25, 25]20Levels$ (b) $t = 1.0$,$[-25, 25]10Levels$

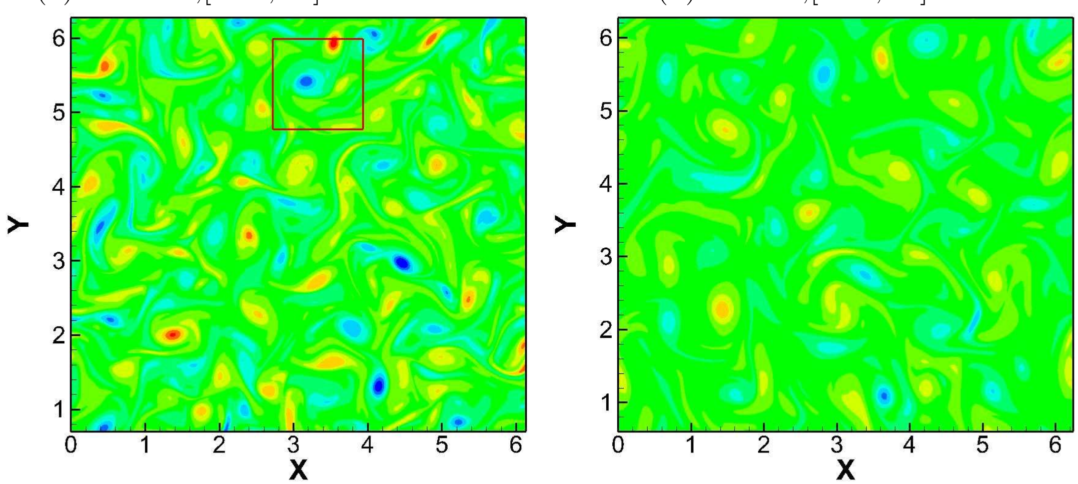

(c) $t = 1.95$,$[-25, 25]10Levels$ (d) $t = 4.0$,$[-25, 25]10Levels$

Figure 23: The time evolution of vorticity in two-dimensional decaying turbulence.

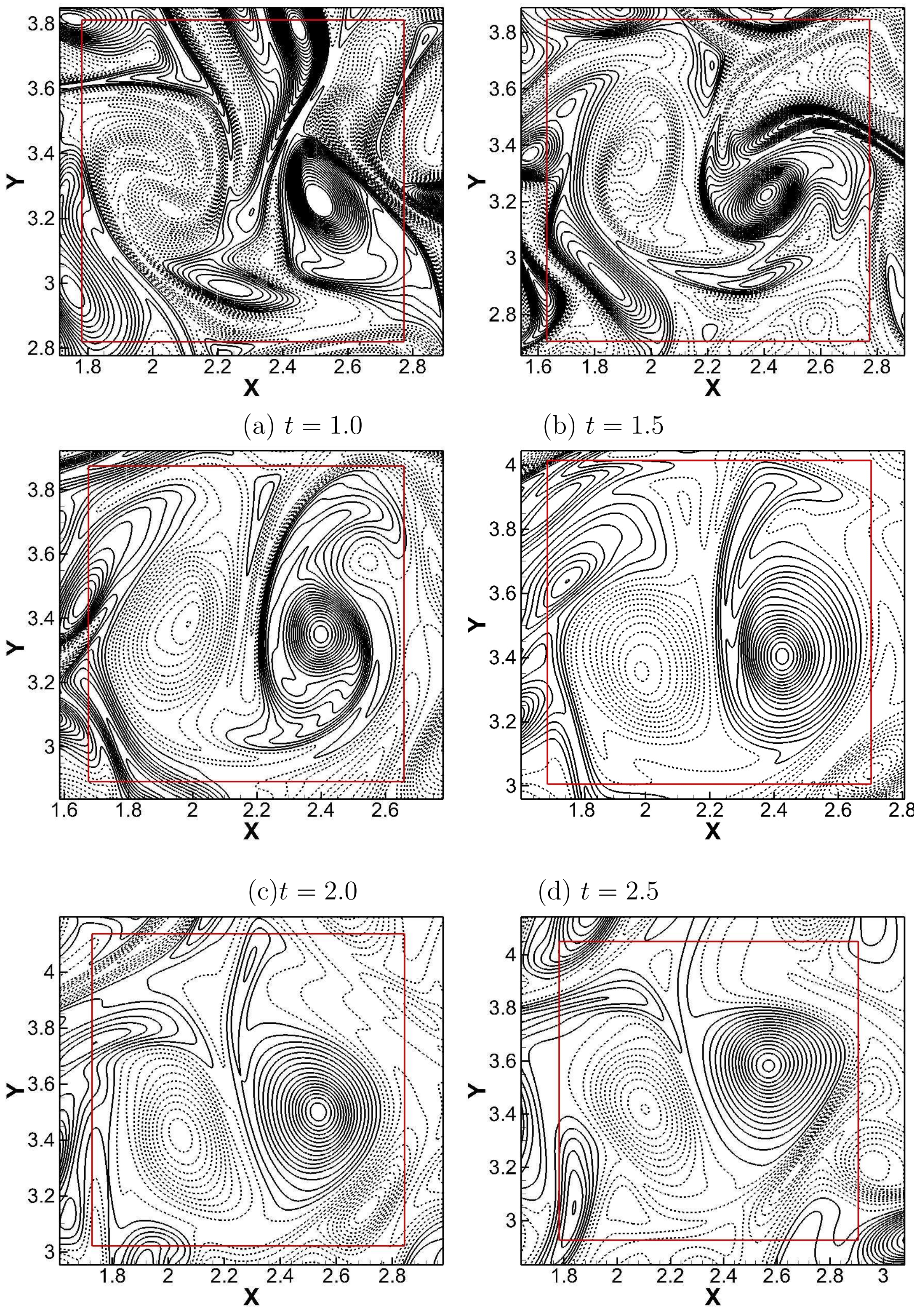

(a) $t = 1.0$ (b) $t = 1.5$

(c) $t = 2.0$ (d) $t = 2.5$

(e) $t = 3.0$ (f) $t = 3.5$

Figure 24: The time evolution of vorticity for vortex dipole in two-dimensional decaying turbulence.

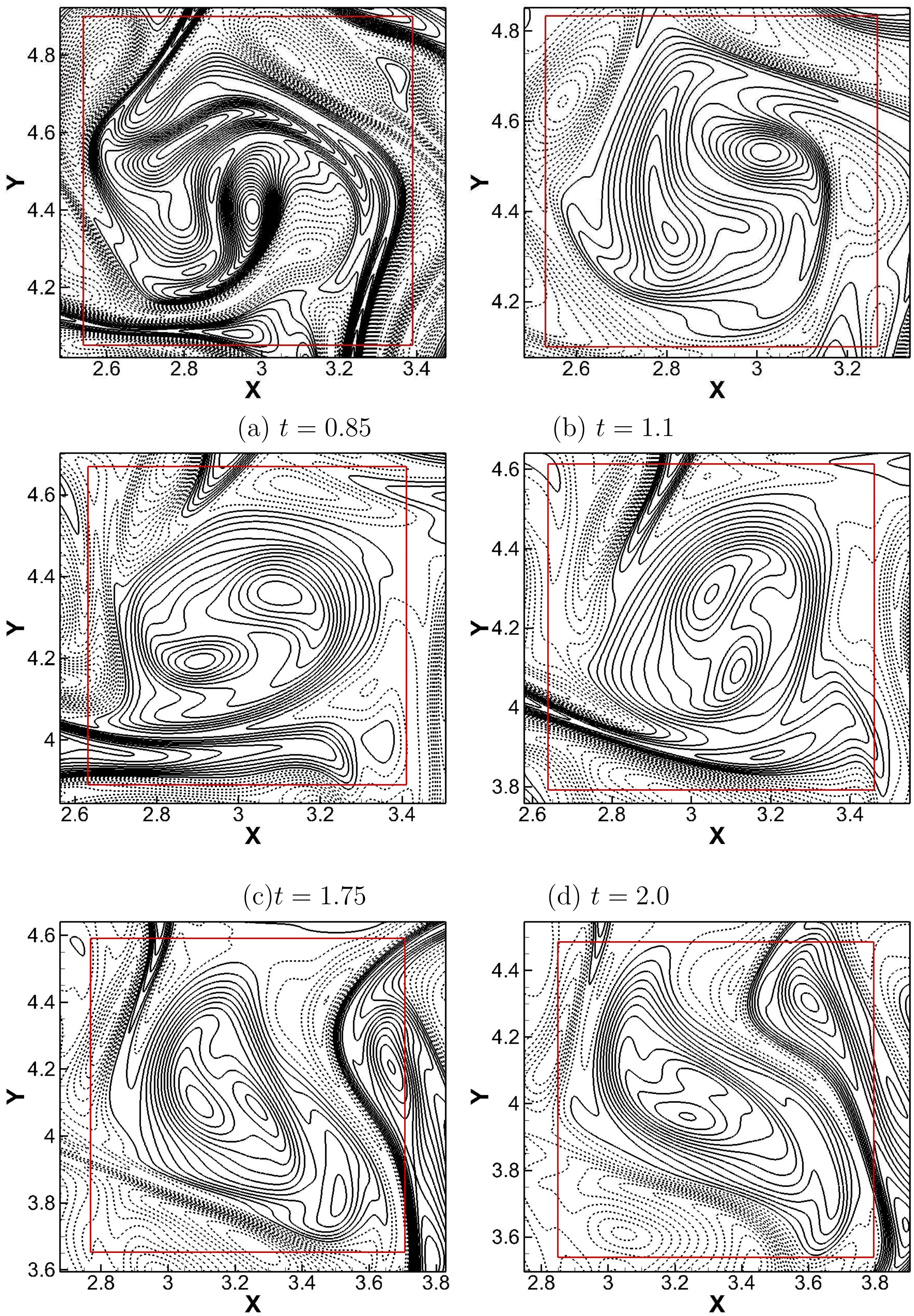

(a) $t = 0.85$ (b) $t = 1.1$

(c)$t = 1.75$ (d) $t = 2.0$

(e)$t = 2.25$ (f) $t = 2.45$

Figure 25: The time evolution of vorticity for vortex merging in two-dimensional decaying turbulence.

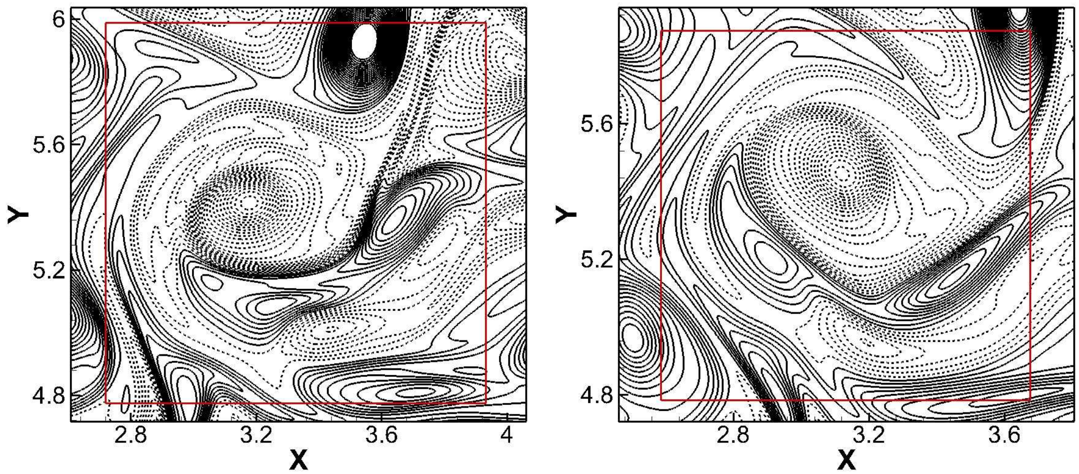

(a) $t = 1.95$ (b) $t = 2.25$

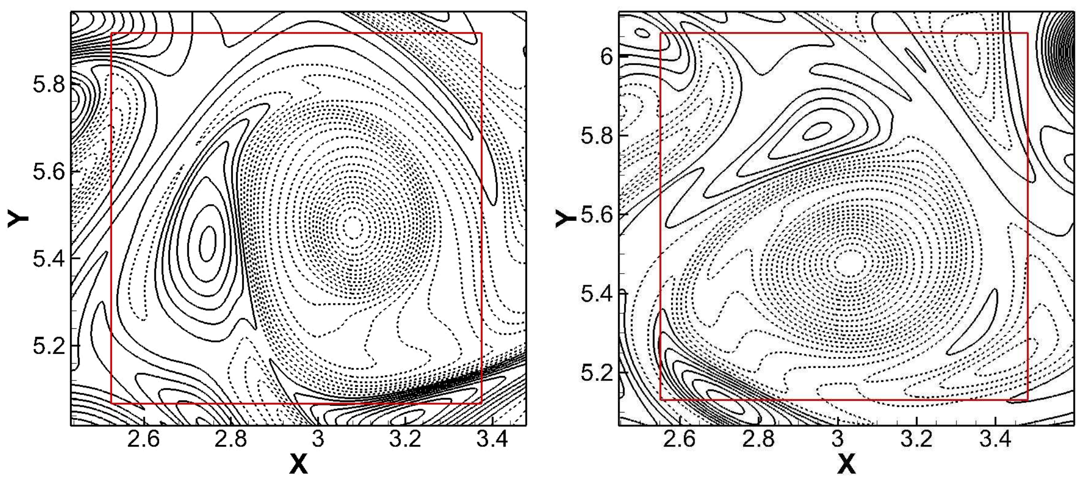

(c)$t = 2.50$ (d) $t = 3.00$

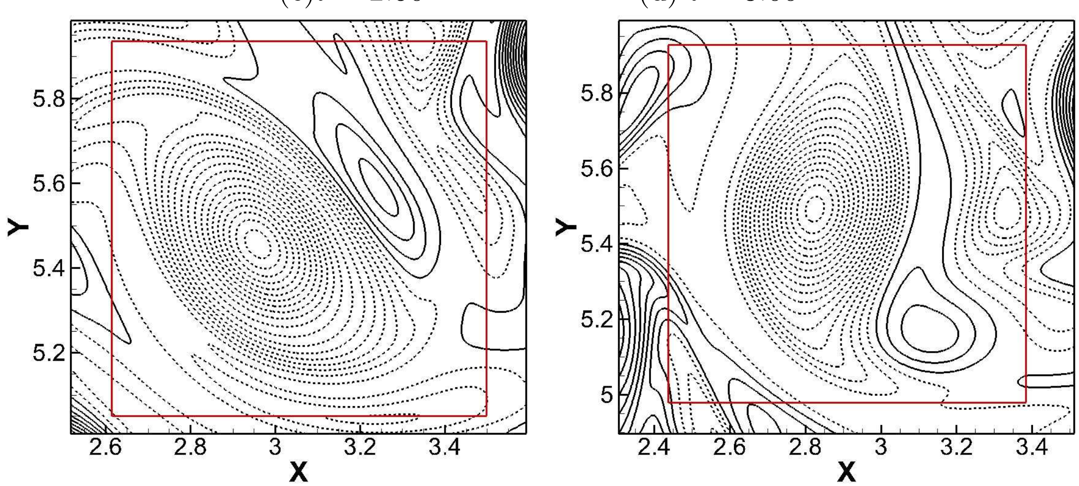

(e)$t = 3.50$ (f) $t = 4.00$

Figure 26: The time evolution of vorticity for the interaction of two vortices with large difference in their strengths in two-dimensional decaying turbulence.

dipoles are formed. One is stronger which results from the inner layer of the initial vortices. The other is weaker which results from the outer layer of the initial vortices. They are advected in opposite directions by the induced velocity.

All other types of interactions result in one or two multi-polar vortex structures which take leapfrogging motion. Under certain specific conditions, two co-rotating vortices will merge together to form a three polar vortex structure. The cores of the two initial vortices merge together to form a stronger vortex core. The outer layers separate from the inner layers and form two weaker vortices near the stronger vortex. The weaker vortices rotate in opposite direction around the stronger vortex. This three polar vortex structure takes a leapfrogging motion.

All four types of interaction can generate sound waves. The distortion is the basic motion of the interaction of two Taylor vortices. The distortion and formation of two vortex dipoles of the interaction of two counter-rotating vortices can generates several sound waves. But the unsteady motions of the vortex dipoles do not generated much sound wave. The distortion and coalescence of two co-rotating vortices can generate high-frequency sound waves with large amplitude, while the leapfrogging of multi-polar vortex structure can generate low frequency sound waves with low amplitude.

Three types of interaction are found in the two dimensional decaying turbulence by direct numerical simulation, which partly demonstrate our classification for the two dimensional interaction of two Taylor vortices.

References

[1] Lighthill M.J. (1952). On sound generated aerodynamically. I. General theory. Proceedings of the Royal Society of London, Series A 221, 564-587.

[2] Powell A. (1964). Vortex sound theory. Journal of the Acoustical Society of America 36, 177-195.

[3] Crow S.C. (1970). Aerodynamic sound emission as a singular perturbation problem. Studies of Applied Mathematics 49, 21-44.

[4] Ffowcs Williams J.E. and Kempton A.J. (1978). The noise from the large-scale structure of a jet. Journal of Fluid Mechanics 84, 673-694.

[5] Doak P.E. (1998). Fluctuating total enthalpy as the basic generalized acoustic field. Theoretical and Computational Fluid Dynamics 10, 115-133.

[6] Lilley G.M. (1972). Generation of sound in a mixing region. Lockheed Aircraft Co. fourth monthly progress report on contract F-33615-71-C-1663, Marietta.

[7] Lilley G.M. (1974). On the noise generation. Noise Mechanism, AGARD-cp-131, 13.1-13.12.

[8] Lilley G.M. (1996). The radiated noise from isotropic turbulence with application to the theory of jet noise. Journal of Sound and Vibration 190, 463-476.

[9] Goldstein M.E. (2003). A generalized acoustic analogy. Journal of Fluid Mechanics 488, 315-333.

[10] Colonius T., Lele S.K. and Moin P. (1997). Sound generation in a mixing layer. Journal of Fluid Mechanics 330, 375-409.

[11] Das I.S., Khavaran A. and Krejsa E.A. (1997). A computational study of contoured plug-nozzle jet noise. Journal of Sound and Vibration 206, 169-194.

[12] Cox J.S., Brentner K.S. and Rumsey C.L. (1998). Computation of vortex shedding and radiated sound for a circular cylinder: subcritical to transcritical Reynolds numbers. Theoretical and Computational Fluid Dynamics 12, 233-253.

[13] Terracol M., Manoha E., Herrero C., Labourasse E., Redonnet S. and Sagaut P. (2005). Hybrid methods for airframe noise numerical prediction Theoretical and Computational Fluid Dynamics 19, 197-227.

[14] Morris P.J. and Zaman K.B.M.Q. (2009). Velocity measurements in jets with application to noise source modeling. AIAA Paper 2009-17.

[15] Morris P.J. and Zaman K.B.M.Q. (2010). Velocity measurements in jets with application to noise source modeling. Journal of Sound and Vibration 239, 394-414.

[16] Morris P.J. and Zaman K.B.M.Q. (2010). Two component velocity correlations in jets and noise source modeling. AIAA Paper 2010-3781.

[17] Prokora C.D. and McGuirk J.J. (2008). Spatio-temporal turbulence correlation using a high speed PIV in an axi-symmetric jet. AIAA Paper 2008-3028.

[18] Mitchell B.E., Lele S.K. and Moin P. (1995). Direct computation of the sound from a compressible co-rotating vortex pair. Journal of Fluid Mechanics 285, 181-202.

[19] Mitchell B.E., Lele S.K. and Moin P. (1999). Direct computation of the sound generated by vortex pairing in an axisymmetric jet. Journal of Fluid Mechanics 383, 113-142.

[20] Wu C. and Wang L. (2009). Numerical simulations of self-propelled swimming of 3D bionic fish school. Science in China Series E, Technological Sciences 52, 658-669.

[21] Wu C. and Wang L. (2010). Where is the rudder of a fish?: the mechanism of swimming and control of self-propelled fish school. Acta Mechanica Sinica 26, 45-69.

[22] Zhang S., Zhang Y.-T. and Shu C.-W. (2006). Interaction of an oblique shock wave with a pair of parallel vortices: Shock dynamics and mechanism of sound generation. Physics of Fluids 18, 126101.

[23] Zhang S., Jiang S., Zhang Y.-T. and Shu C.-W. (2009). The mechanism of sound generation in the interaction between a shock wave and two counter-rotating vortices. Physics of Fluids 21, 076101.

[24] Tang S.K. and Ko N.W.M. (2000). Sound sources in the interactions of two inviscid two-dimensional vortex pairs. Journal of Fluid Mechanics 419, 177-201.

[25] Tang S.K. and Ko N.W.M. (2001). Mechanism for sound generation in inviscid two-dimensional vortex interactions. Journal of Sound Vibration 243, 823-846.

[26] Möhring W. (1978)On vortex sound at low Mach number. Journal of Fluid Mechanics 85, 685-691.

[27] Eldredge J.D. (2007). The dynamics and acoustics of viscous two-dimensional leapfrogging vortices. Journal of Sound and Vibration 301, 74-92.

[28] Dosanjh D.S. and Weeks T.M. (1965). Interaction of a starting vortex as well as a vortex street with a traveling shock wave. AIAA Journal 3, 216-223.

[29] Weeks T.M. and Dosanjh D.S. (1967). Sound generation by shock-vortex interaction. AIAA Journal 5, 660-669.

[30] Ellzey J.L. and Henneke M.R. (1997). The shock-vortex interaction: the origins of the acoustic wave. Fluid Dynamics Research 21, 171-184.

[31] Zhang S., Zhang Y.-T. and Shu C.-W. (2005). Multistage interaction of a shock wave and a strong vortex. Physics of Fluids 17, 116101.

[32] Pirozzoli S., Grasso F. and D'Andrea A. (2001). Interaction of a shock wave with two counter-rotating vortices: Shock dynamics and sound production. Physics of Fluids 13, 3460-3481.

[33] Chatterjee A. and Vijayaraj S. (2008). Multiple sound generation in interaction of shock wave with strong vortex. AIAA journal 46, 2558-2567.

[34] Jiang G.-S. and Shu C.-W. (1996). Efficient implementation of weighted ENO schemes. Journal of Computational Physics 126, 202-228.

[35] Shu C.-W. (1998). Essentially non-oscillatory and weighted essentially non-oscillatory schemes for hyperbolic conservation laws. In *Advanced Numerical Approximation of*

Nonlinear Hyperbolic Equations, B. Cockburn, C. Johnson, C.-W. Shu and E. Tadmor (Editor: A. Quarteroni), Lecture Notes in Mathematics, volume 1697, Springer, Berlin, 325-432.

[36] Shu, C.-W. and Osher, S. (1988), Efficient implementation of essentially non-oscillatory shock capturing schemes. J. Comput. Phys. 77, 439-471.

[37] Inoue O. and Hattori Y. (1999). Sound generation by shock-vortex interactions. Journal of Fluid Mechanics 380, 81-116.

[38] Grasso F. and Pirozzoli S. (2001). Simulations and analysis of the coupling process of compressible vortex pair: Free evolution and shock induced coupling. Physics of Fluids 13, 1343-1366.

[39] Schmidt M.R., Beckers M., Nielsen A.H., Rasmussen J. Juul and Heijst G.J.F. van (1998). On the interaction between two oppositely signed, shielded, monopolar vortices. Physics of Fluids 12, 3099-3110.

[40] Cerretelli C. and Williamson C.H.K. (2003). The physical mechanism for vortex merging. Journal of Fluid Mechanics 475, 41-77.

[41] Melander M.V., Zabusky N.J. and Mcwilliams J.C. (1988). Symmetric vortex merger in two dimensions: causes and conditions. Journal of Fluid Mechanics 195, 303-340.

[42] Colonius T., Lele S. K. and Moin P. (1994). The scattering of sound waves by a vortex:numerical simulations and analytical solutions. Journal of Fluid Mechanics 260, 271-298

[43] Eldredge J.D., Colonius T. and Leonard A. (2002). A vortex particle method for two dimensional compressible flow. Journal of Computational Physics 179, 371-399

[44] San O. and Staples A.E. (2012). High-order methods for decaying two-dimensional homogeneous isotropic turbulence. Computers & Fluids, 63, 105-127.

[45] Boffetta G. and Ecke R.E. (2012). Two-dimensional turbulence. Annual Review of Fluid Mechanics 44, 427-451.

[46] Keetels G.H., Clercx H.J.H. and Van Heijst G.J.F. (2010). On the origin of spin-up processes in decaying two-dimensional turbulence. European Journal of Mechanics B/Fluids 29, 1-8.

[47] Xiao Z., Wan M., Chen S. and Eyink G.L. (2008). Physical mechanism of the inverse energy cascade of two-dimensional turbulence: a numerical investigation. Journal of Fluid Mechanics 619, 1-44.